JGR Earth Surface

RESEARCH ARTICLE
10.1029/2022JF006907

Magnesium Isotope Constraints on the Holocene Hydromagnesite Formation in Alkaline Lake Dujiali, Central Qinghai-Tibetan Plateau

Yongjie Lin[1,2], William J. Knapp[2], Weiqiang Li[3], Mianping Zheng[1], Chuanyong Ye[1], Jiaxin She[3], Zhiguang Xia[3], Ian M. Power[4], Yue Zhao[1], and Edward T. Tipper[2]

[1]MNR Key Laboratory of Saline Lake Resources and Environments, Institute of Mineral Resources, Chinese Academy of Geological Sciences, Beijing, China, [2]Department of Earth Sciences, University of Cambridge, Cambridge, UK, [3]State Key Laboratory for Mineral Deposits Research, School of Earth Sciences and Engineering, Nanjing University, Nanjing, China, [4]Trent School of the Environment, Trent University, Peterborough, ON, Canada

Key Points:

- New Mg isotope data on Holocene hydromagnesite, modern lake, and river waters from the alpine Dujiali Lake, central Qinghai-Tibetan Plateau
- A thermodynamic based box model simulates the behavior of the carbonate system and Mg isotopes during the evolution of the lake chemistry
- Low-Mg carbonate precipitation may be a common precursor process for driving hydromagnesite precipitation in evaporative alkaline lakes

Supporting Information:

Supporting Information may be found in the online version of this article.

Correspondence to:

Y. Lin and E. T. Tipper,
linyongjie2014@163.com;
ett20@cam.ac.uk

Citation:

Lin, Y., Knapp, W. J., Li, W., Zheng, M., Ye, C., She, J., et al. (2023). Magnesium isotope constraints on the Holocene hydromagnesite formation in alkaline Lake Dujiali, central Qinghai-Tibetan Plateau. *Journal of Geophysical Research: Earth Surface*, *128*, e2022JF006907. https://doi.org/10.1029/2022JF006907

Received 4 SEP 2022
Accepted 5 FEB 2023

Author Contributions:

Conceptualization: Yongjie Lin, Weiqiang Li, Edward T. Tipper
Formal analysis: Weiqiang Li, Jiaxin She, Zhiguang Xia
Funding acquisition: Yongjie Lin, Edward T. Tipper
Investigation: Chuanyong Ye
Methodology: Yongjie Lin, William J. Knapp, Weiqiang Li, Edward T. Tipper

Abstract Hydromagnesite ($Mg_5(CO_3)_4(OH)_2 \cdot 4H_2O$) is a common hydrated magnesium carbonate mineral found in alkaline lakes on Earth, potentially present on Mars, and is also a key mineral for carbon capture and storage. However, mechanisms governing its formation in alkaline lakes remain enigmatic. Extensive hydromagnesite formed during the Holocene in the alkaline Dujiali Lake (DL), central Qinghai-Tibetan Plateau, making it an ideal field site to constrain the process of hydromagnesite formation in a modern environmental context. In this study, we report a set of magnesium isotope ratios ($^{26}Mg/^{24}Mg$ expressed as δ^{26} Mg) data from DL on abiotic hydromagnesite (mean = −1.35‰ ± 0.14‰) modern lake waters (−0.07‰ to +0.46‰), and rivers and groundwater (−0.53‰ to −1.46‰). These differences in δ^{26} Mg (and also Mg/Ca) are most likely caused by low-Mg carbonate precipitation, a process which fractionates Mg/Ca and $\delta^{26}Mg$ values. A semi-quantitative box model of the lake chemistry was developed based on carbonate equilibria to investigate the behavior of Mg isotopes during the evolution of the lake chemistry. The modeling results indicate that evaporation concentrates solutes in the lake driving saturation of multiple minerals. Aragonite reaches saturation before hydromagnesite, preferentially removing Ca relative to Mg via aragonite precipitation. This process elevates the Mg/Ca of the lake and the saturation index of hydromagnesite, increasing the likelihood of hydromagnesite formation. Given that the Mg/Ca ratio of many alkaline lakes is far below than that required for the formation of hydromagnesite, our findings suggest that low-Mg carbonate precipitation may be a common precursor process for abiotic hydromagnesite precipitation in evaporative environments in addition to a high Mg source likely derived from ultramafic rocks.

Plain Language Summary Hydromagnesite ($Mg_5(CO_3)_4(OH)_2 \cdot 4H_2O$) is a common hydrated magnesium carbonate mineral on the Earth and is suspected to be present at the Jezero Crater on Mars. Hydromagnesite formation requires high Mg/Ca ratios, typically associated with the weathering of ultramafic rocks. However, the Mg/Ca ratios of the input waters associated with ultramafic rocks in most of the settings are seldom high enough for hydromagnesite precipitation in alkaline lakes. Our study suggests that although ultramafic Mg source rocks are important for hydromagnesite precipitation, the removal of Ca through Ca-carbonate formation is an essential precursor process for increasing the Mg/Ca ratio under intense evaporation conditions to induce spontaneous hydromagnesite precipitation.

1. Introduction

Magnesium (Mg) is approximately 30 times more abundant than calcium (Ca) at a planetary scale (Allegre et al., 1995). While Ca carbonates form one of the planet's largest carbon reservoirs, the precipitation of anhydrous Mg carbonate (e.g., magnesite) is extremely slow at ambient temperatures due to the strong hydration energy of aqueous magnesium (Saldi et al., 2009). Hydromagnesite ($Mg_5(CO_3)_4(OH)_2 \cdot 4H_2O$) is more common in natural terrestrial environments (Braithwaite & Zedef, 1996; Lin et al., 2017; Oskierski et al., 2021; Power et al., 2009, 2014, 2019; Wilson et al., 2006), and is potentially present in Jezero crater, Mars (Horgan et al., 2020; Scheller et al., 2021). Interest in hydromagnesite is growing due to its potential capacity to store CO_2 by mineral carbonation (Oskierski et al., 2021; Wilson et al., 2006) and a detailed understanding of the formation mechanisms of hydromagnesite are required to exploit the potential of mineral carbonation.

Writing – original draft: Yongjie Lin, William J. Knapp, Weiqiang Li, Edward T. Tipper
Writing – review & editing: Yongjie Lin, William J. Knapp, Weiqiang Li, Mianping Zheng, Chuanyong Ye, Jiaxin She, Zhiguang Xia, Ian M. Power, Yue Zhao, Edward T. Tipper

Hydromagnesite is common in (a) altered ultramafic rocks (Oskierski et al., 2021; Wilson et al., 2006), (b) as an authigenic mineral in alkaline lakes and playas (Braithwaite & Zedef, 1996; Chagas et al., 2016; Power et al., 2009; Zeyen et al., 2021), and (c) in karstic cave systems as speleothems and "moonmilk" (Broughton, 1972; Canaveras et al., 1999). Hydromagnesite is typically associated with high aqueous Mg/Ca ratios and high alkalinity ($HCO_3^- + CO_3^{2-}$) (Braithwaite & Zedef, 1996; Chagas et al., 2016; Lin et al., 2017; Power et al., 2009; Zeyen et al., 2021). Hydromagnesite formation in a natural setting has been directly linked to the Mg/Ca ratios of formation waters (Chagas et al., 2016; Fischbeck & Müller, 1971; Zeyen et al., 2021). In alkaline lakes, a high Mg/Ca ratio (e.g., >39; mol/mol) is always required for hydromagnesite formation (Chagas et al., 2016), even when the hydromagnesite is microbially mediated (Power et al., 2009; Shirokova et al., 2013). An even higher Mg/Ca ratio is required for hydromagnesite formation in laboratory settings (Sun et al., 2002; P. Zhang et al., 2021), and low-temperature thermodynamic calculations (Königsberger et al., 1999). Alkaline lakes and playas associated with hydromagnesite formation are usually associated with water inputs dissolving mafic and ultramafic rocks (Braithwaite & Zedef, 1996; Power et al., 2009; Zeyen et al., 2021). The dissolution of mafic and ultramafic rocks is thought to provide an abundant source of Mg, but the Mg/Ca ratios of waters draining mafic and ultramafic rocks are not always high enough for hydromagnesite formation (Last et al., 2010). High Mg/Ca ratios are atypical of terrestrial fresh waters. There are few experimental studies demonstrating direct hydromagnesite nucleation at Earth surface temperatures (Berninger et al., 2014; Gautier et al., 2014). Therefore, many studies emphasized the potential role of microbes in mediating hydromagnesite formation in alkaline lakes (Power et al., 2009, 2014, 2019; Sanz-Montero et al., 2019; Zeyen et al., 2021). Power et al. (2007, 2019) proposed hydromagnesite may be transformed from the more hydrated Mg-carbonates dypingite. Alternatively, an amorphous magnesium carbonate phase could possibly serve as precursor for hydromagnesite crystallization (Fukushi & Matsumiya, 2018; Zeyen et al., 2021). Consequently, hydromagnesite formation processes in alkaline lake environments remains under-constrained.

Mg isotopes are an emerging geochemical tracer that are known to fractionate during precipitation of carbonates and silicates from aqueous fluids, and are thus useful for quantifying carbonate precipitation processes (Harrison et al., 2021; Hindshaw et al., 2020; Li et al., 2012; Mavromatis et al., 2021; Oelkers et al., 2018; Tipper, 2022; Tipper et al., 2006a, 2008). In this study, we present Mg isotope data ($\delta^{26}Mg/^{24}Mg$ expressed as $\delta^{26}Mg$ in per mil units) and Mg/Ca data on lake waters, incoming stream and groundwaters, lake sediments, and related hydromagnesite in the well-studied alkaline Dujiali Lake (DL) in Tibet (Lin et al., 2017, 2019a, 2019b), and compare these to global databases of waters and other alkaline lakes where hydromagnesite forms. DL is undersaturated with respect to hydromagnesite in the present day, but in the recent past (Holocene), substantial volumes of hydromagnesite have been deposited from DL. We show that the modern input waters to the lake have low Mg/Ca ratios typical of global databases of rivers. Combined with a box model of the lake chemistry we investigate the behavior of the carbonate system and $\delta^{26}Mg$ during the evolution of the lake chemistry to suggest why hydromagnesite does not precipitate in the modern environment but did precipitate in the Holocene. We show that the evaporation drives the alkalinity and the Mg/Ca ratio of lake waters to increase via low-Mg carbonate precipitation (e.g., aragonite), eventually driving the supersaturation of abiotic hydromagnesite. Mg isotope ratios provide a unique constraint on the precipitation parameters. Our results identify a mechanism for the formation of hydromagnesite that contributes to an improved understanding of hydromagnesite formation in natural settings. The experimental and modeling protocol provides opportunities for calibrating the chemical conditions of hydromagnesite formation in alkaline lakes.

2. Site Description

DL is located in the central Qinghai-Tibet Plateau (QTP; Figure 1, China, 4,524 m above sea level) (Lin et al., 2017, 2019a, 2019b). It formed as a subsiding sub-basin located within a larger Cenozoic faulted basin that comprises neighboring Lake Selin Co (Siling Lake or Qilin Lake, the largest lake in Tibet). The modern lake has a surface area of 80 km^2 and is approximately 3 m deep. Geomorphologically, the DL basin is characterized by multi-stepped terraces covered by Quaternary sediments, a heterogeneous mixture of gravel, sand, silt, clay, and salt deposits (Zheng et al., 2002). There are limestones, andesite, mudstone, and coarse-grained clastic sediments surrounding the lake, but few ultramafic rocks at the surface in the vicinity of DL (Lin et al., 2017; Zheng et al., 2002). The chemistry of input waters is thought to be influenced by dissolution of ultramafic minerals based on the distribution of rare earth elements (Lin et al., 2019a). The lake-bed is known to have been dry in the 1980s with the present water volume and solute mass having accumulated since that time. Significant lake

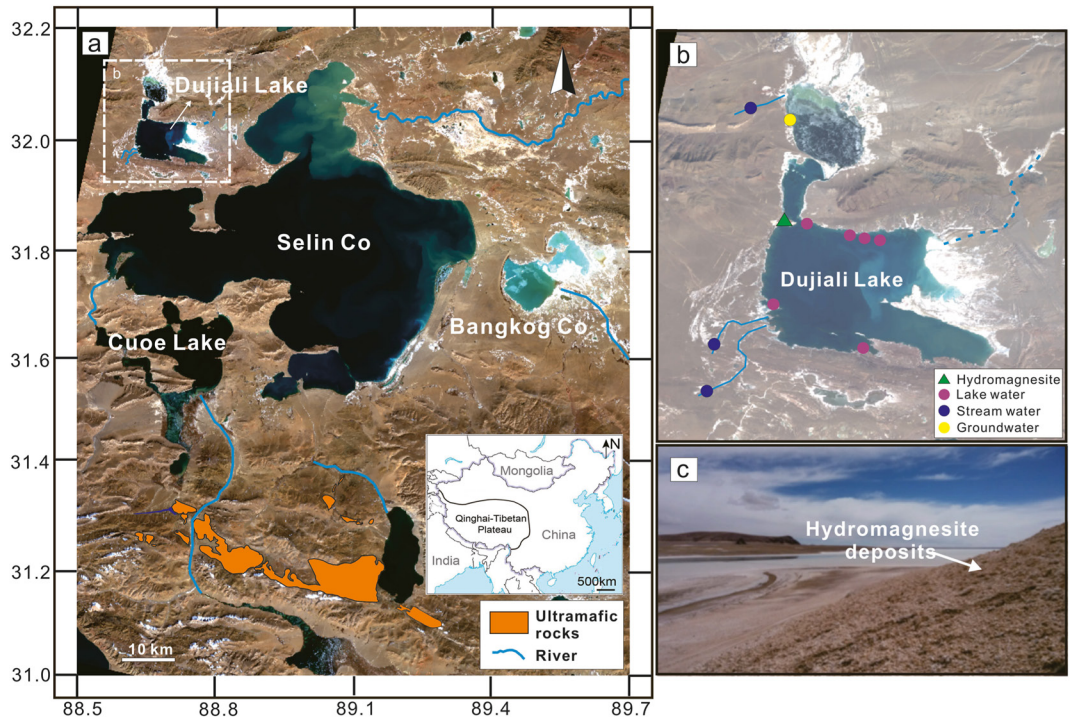

Figure 1. (a) Satellite map (from https://earthexplorer.usgs.gov/) for the area surrounding Dujiali Lake (DL), showing nearby lakes where hydromagnesite deposits are found. The distribution of ultramafic rocks is shown. (b) Zoomed-in area of DL showing sample locations, and (c) photo of the hydromagnesite deposit.

expansion has occurred in QTP in recent decades (Liu et al., 2021), including DL, due to the increase of precipitation and meltwater from ice. DL has not been connected to any of the neighboring lakes in the Holocene (Zheng et al., 2002).

The climate is cold continental, sub-humid to semi-arid with an annual mean temperature of 0°C (range of −22 to 17°C). DL is frozen in winter for around 5 months each year (November to March). The mean precipitation is < 200 mm and the mean evaporation is 2,400 mm (Zheng et al., 2002). This resulting moisture deficit helps maintain the elevated salinities of most of the lakes in the QTP. DL is a closed endorheic basin that is primarily recharged by meteoric water and seasonal rivers with no visible evidence of groundwater recharge (Zheng et al., 2002). At the present day, the hydrochemistry of the lake is alkaline (pH = 9.37) and carbonate-dominated. Total dissolved solids (TDS) are 1.5–9.3 g/L with Na^+, K^+, Mg^{2+}, SO_4^{2-}, HCO_3^-, CO_3^{2-}, and $B_4O_7^{2-}$ being the dominant ions (Lin et al., 2017).

DL is one of the few modern environments on the Earth's surface where there has been extensive hydromagnesite precipitation during the Holocene. Hydromagnesite deposits were distributed in bands around the margins and within the lake, which is thought to have periodically dried to form a playa. The Holocene hydromagnesite deposits occur in the first lake terrace in the northwest of the lake (Figure 1) and formed between 6090 ± 25 Cal a BP to 5835 ± 30 Cal a BP (Lin et al., 2017). These deposits are up to 6 m thick above the present lake surface and are parallel to the current local topography (Figure 1c). Carbon isotope measurements ($\delta^{13}C$) from the hydromagnesite appear to vary systematically across the vertical thickness of the hydromagnesite deposit, suggesting the hydromagnesite might have formed as one continuous depositional event rather than multiple episodes of periodic drying (Lin et al., 2017). The precipitation of hydromagnesite is believed to be an inorganic process at DL, with the dissolved inorganic carbon that contributes to the hydromagnesite thought to originate primarily from the atmosphere (Lin et al., 2017). The hydromagnesite directly overlays Quaternary sediments and is distributed in an east-west direction, with a length of about 2 km and a width of about 0.3 km. The hydromagnesite sediments are bright-white, dry, and clay-like with a weathered surface crust. The deposits are mostly hydromagnesite (wt.% 95%–98%), with aragonite (wt.% 2%–5%), as determined by X-ray diffraction (XRD) and X-ray fluorescence (XRF) analyses (Lin et al., 2019b).

3. Material and Analytical Methods

3.1. Sample Collection and Description

Twenty-six hydromagnesite samples were collected equidistantly from different horizons of the hydromagnesite deposit after the removal of the weathered surface crust and numbered 1 (bottom) to 26 (top) in March 2015. In addition, three lake sediments were collected from the lake bottom. The lake sediments were collected from different locations of the lake at various depths using a Shaw backpack core drilling mechanism. The lake sediment sample DJZS01 was collected from the lake bottom at 40 cm sediment depth under 200 cm of lake water beneath a 30 cm ice layer in the eastern part of the lake. The lake sediment sample DJZS06 was collected from the lake bottom with 10 cm sediment depth, under 40 cm depth lake water beneath a 10 cm-thick ice layer in the southern part of the lake. The lake sediment sample DJZS05 was collected from the surface of the lake bottom under a 30 cm-thick ice layer in the northern part of the lake.

Three stream water samples and one groundwater sample were collected from inflowing streams and the lake littoral zone (Figure 1). The groundwater DJS01 was collected from a 10 m deep well close to the lake. Stream water DJS02 flowed from an alluvial fan flowing into the north of the lake. Stream water DJS03 is supplied by glacial meltwater from distant glaciers. Stream water DJS04 recharges the lake that flowed through an alluvial fan in the southwest of the lake (Qu et al., 2011). At the time of sampling, there were no other streams observed to be supplying water to the lake. However, geomorphologically a dry stream channel was observed in the northwest region of the lake that is thought to flow in times of seasonal meltwaters. Six lake waters were collected after breaking the ice on the lake. All water samples were filtered on collection (0.45 μm nylon membrane filters) at the field site into polyethylene bottles that were pre-rinsed with each filtered water sample, with no head space. These samples were transferred to the hydrochemistry laboratory in the Institute of Mineral Resources, CAGS, and stored at 4°C until analysis.

3.2. Characterisation of Solid and Water Samples

The mineralogy of hydromagnesite deposits and lake sediments was determined by XRD using an X-ray diffractometer (TTR-3, Rigaku Corp, Tokyo, Japan). The XRD was operated at 45 kV and 30 mA and used Cu Kα radiation ($\lambda = 1.54056$ Å). To constrain clay mineralogy, XRD on the clay mineral fractions (<2 μm) of lake sediments powders was conducted on both the air-dried oriented clay sample (N), ethylene glycol-saturated clay sample (EG), and 550°C heated clay sample (*T*). The clay fraction (<2 μm) was separated from dried lake sediments by centrifuging suspensions in distilled water and decanting the supernatant and drying at 40°C. The mineral compositions and their relative proportions of the bulk rocks and clay minerals in the purified clay samples were obtained using the Clayquan (2016 version) program with Rietveld refinements methods. The relative analytical error is ±5%. The major element compositions of lake sediments were determined using XRF spectrometry. Fusion glasses were prepared by mixing the sample with an alkaline flux ($Li_2B_4O_7$) in the proportion 1:8. The analytical precision was better than 5% for repeated analyses. Chinese national rock standards were used for calibration. Loss on ignition was determined by weighing samples before and after 1 hr of heating at 1075 ± 25°C.

The concentration of major elements except for silicon (as H_4SiO_4) for all the water samples were analyzed and reported by Lin et al. (2017, 2019a). The dissolved silicon concentrations of water samples were carried out at Nanjing FocuMS Technology Co. Ltd. using ICP-OES (Agilent 5110). The standard solution was prepared from China standard GSBG 62007-90 (1401) and was treated as quality control. The analytical precision was better than 5% for repeated analyses.

3.3. Mg Isotope Analytical Methods

Stream, groundwater, lake water samples, dissolved hydromagnesite samples, and the digestions of the bulk lake sediment of lake sediments were analyzed for Mg isotope ratios. About 10 mg of hydromagnesite powders were dissolved using 1 mL 1 M HNO_3 in perfluoroalkoxy alkane beakers at room temperature overnight, then diluted in 5 mL deionized water. A 0.1 ml aliquot of the solution was diluted to 5 mL for elemental concentration measurement using ICP-OES. Chemical separation and Mg isotope analyses of the selected liquid and solid samples were performed at the State Key Laboratory for Mineral Deposits Research of Nanjing University following the protocol described by Hu et al. (2017). Based on the measured Mg content, an aliquot of each

sample solution (liquid samples and dissolved bulk sample powders) that contained 50 μg Mg was processed to separate Mg from the matrix elements. Samples were firstly loaded onto a quartz glass column containing 1 mL Biorad cation exchange resin AG50W-X12 (100–200 mesh). On the second column, samples were loaded onto a custom-made Teflon column containing 0.2 mL Biorad cation exchange resin AG50W-X8 (100–200 mesh). More than 99% of the initial Mg was recovered after these two column treatments, and the matrix elements were less than 1% of Mg. The total procedural blank was estimated as less than 30 ng for Mg (Xia et al., 2020). USGS igneous rock standards (DTS-2) and IAPSO seawater were treated as unknown samples for column purification to monitor the chemical separation process and verify the accuracy of the method. Mg isotopic compositions were analyzed on Thermo Fisher Scientific Neptune Plus MC-ICP-MS with the sample-standard bracketing method at low-mass-resolution mode, using a 100 μL/min self-aspirating Glass Expansion nebulizer and an SIS glass spray chamber. Samples were analyzed bracketed by an in-house Mg standard (Lot No. HPS909104). The concentration of samples matched the in-house standard to within 10%. The δ^{26}Mg of the in-house standard was determined as $-0.67‰ \pm 0.1‰$ relative to international standard DSM3 (Li et al., 2011, 2019). All Mg isotopic data were normalized to DSM3 using conventional delta notation to express per thousand deviations from DSM3:

$$\delta^{26}\mathrm{Mg}(‰) = \frac{(^{26}\mathrm{Mg}/^{24}\mathrm{Mg})_{\mathrm{sample}} - (^{26}\mathrm{Mg}/^{24}\mathrm{Mg})_{\mathrm{DSM3}}}{(^{26}\mathrm{Mg}/^{24}\mathrm{Mg})_{\mathrm{DSM3}}} \times 1,000 \quad (1)$$

A 40 s on-peak acid blank was measured before each analysis and typical instrument backgrounds were 0.5 mV. Before the sample analysis, the mono-elemental international standards Cambridge-1 and DSM3 were measured to verify the accuracy of our Mg isotope measurements (DSM3 = $0.03 \pm 0.11‰$, 2SD, $n = 2$ and Cambridge-1 = $-2.59‰ \pm 0.04‰$, 2SD, $n = 2$). Both δ^{26}Mg and δ^{25}Mg are reported. The slope between δ^{26}Mg and δ^{25}Mg on a three-isotope plot (Figure S1 in Supporting Information S1) is 0.515, which is intermediate between the theoretical equilibrium and kinetic fractionation lines (Young et al., 2002). The typical reproducibility of δ^{26}Mg for individual samples based on averages of replicate analyses is 0.07‰. The long-term external reproducibility (2SD) was assessed from six replicates of IAPSO seawater through chemistry yielding $\delta^{26}\mathrm{Mg} = -0.80‰ \pm 0.07‰$. DTS-2 yielded a $\delta^{26}\mathrm{Mg} = -0.31‰ \pm 0.11‰$. The absolute values of these standards are within the uncertainty of other laboratories and previous studies (Tipper et al., 2006a, 2006b). Where the uncertainty of an individual sample is lower than the external reproducibility determined by replicates through chemistry, the external uncertainty should be applied.

3.4. Sr Isotope Analytical Methods

The Sr isotope data of water samples discussed in the present study were previously reported in Lin et al. (2019a). Since Mg isotopes were measured on the same samples, the data is discussed again in the context of the new Mg isotope data in the present study. In this study, three dissolved lake sediments samples and an aliquot of the digested and leached samples were dried down and converted to nitrate form by drying in 0.5 ml HNO_3, re-dissolved in 3.5 M HNO_3 for ion exchange purification. Strontium was separated using a cation exchange procedure using 100–200 mesh AG50W-X8 resin. The column was repeated to ensure complete separation of Ca. $^{87}Sr/^{86}Sr$ ratios were determined on a Finnigan Triton Thermo ionization mass spectrometer. $^{87}Sr/^{86}Sr$ ratios were corrected for mass fractionation by normalizing to $^{86}Sr/^{88}Sr = 0.1194$ with an exponential law. Repeated measurements of Sr standard NBS987 yielded $^{87}Sr/^{86}Sr = 0.710259 \pm 0.000015$ (2SD).

4. Results

4.1. Mineralogy and Geochemistry of Hydromagnesite and Lake Sediments

XRD measurements of the Holocene hydromagnesite reveal aragonite is a minor phase (<5%; Table S1 in Supporting Information S2, Figure 2). The δ^{26}Mg values of the hydromagnesite samples (a mixture of aragonite and hydromagnesite) are homogenous (mean = $-1.35‰ \pm 0.14‰$, 2SD, Table S2 in Supporting Information S2) and lower than δ^{26}Mg values of modern lake waters (mean = $-0.16‰$, see below). A similar offset between contemporary hydromagnesite and associated waters has been observed in other lakes, playas, and synthetic hydromagnesite (Mavromatis et al., 2021; Oelkers et al., 2018; Shirokova et al., 2013). The modern lake sediments are comprised of clay minerals, quartz, K-feldspar, calcite, and dolomite with no hydromagnesite (Table S1 in Supporting Information S2). The clay minerals consist mainly of Illite and I/S, with minor kaolinite

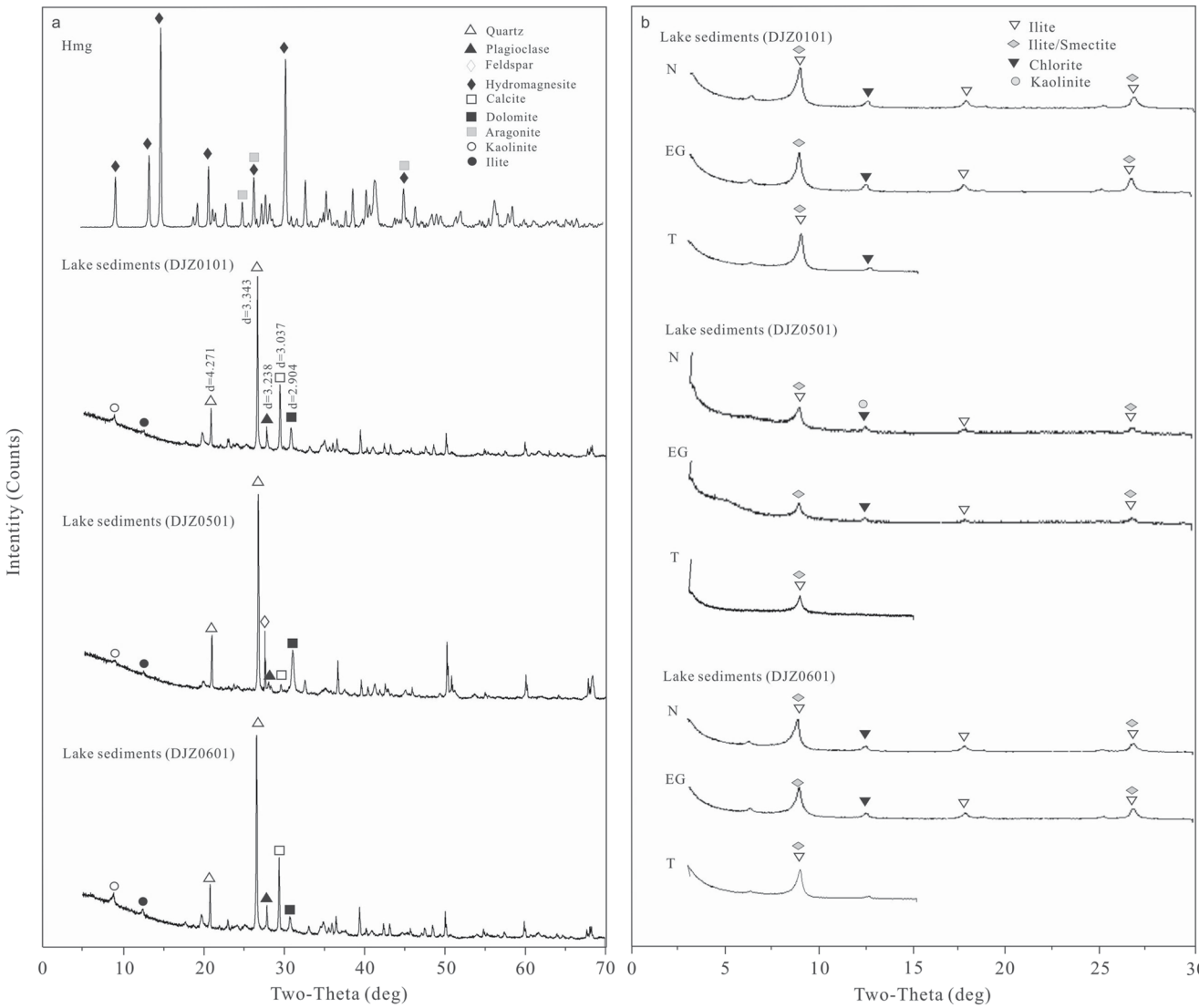

Figure 2. X-ray diffraction (XRD) patterns of the studied hydromagnesite samples and modern lake sediments from Dujiali Lake. (a) Bulk samples; (b) the diffraction pattern of clay minerals. N, Air-dried oriented clay samples; EG, Ethylene glycol-saturated clay samples; T, clay samples post-heating to 550°C.

and chlorite (Figure 2). The $^{87}Sr/^{86}Sr$ ratios of the bulk sediment are very different from the modern lake waters, streams, and hydromagnesite (see below). The calcite and dolomite may be authigenic in origin. The hydromagnesite crystals are plate-like in morphology with no conclusive evidence of microbe, submicron to several microns in width, and ~100 nm in thickness (Figure 3). The $\delta^{26}Mg$ of bulk lake sediments ranges from −0.22‰ to −0.66‰ but because these are bulk measurements cannot be related to the contemporary lake waters because they likely contain detrital minerals.

4.2. Water Chemistry

The Mg contents of the stream and groundwaters are high (0.367–2.425 mmol/L, Table S3 in Supporting Information S2), but their Mg/Ca molar ratios (range of 0.2–2.6) are lower than the modern lake water (range of 2.7–6.8). This is typical of many other stream and lake waters (Figure 4a). Literature data of Mg/Ca ratios from rivers draining different rock types were compiled from the GloRICH data base (Hartmann et al., 2014) to assess the impact of lithology on the Mg/Ca ratio (Table S4 in Supporting Information S2). The Mg/Ca ratio of natural waters increases as the proportion of mafic and ultramafic rocks in a catchment increases (Figure 4, means of 0.9, 1.1, and 9.6, for catchments draining <15% mafic rocks, >85% mafic rocks, and mono-lithological ultramafic

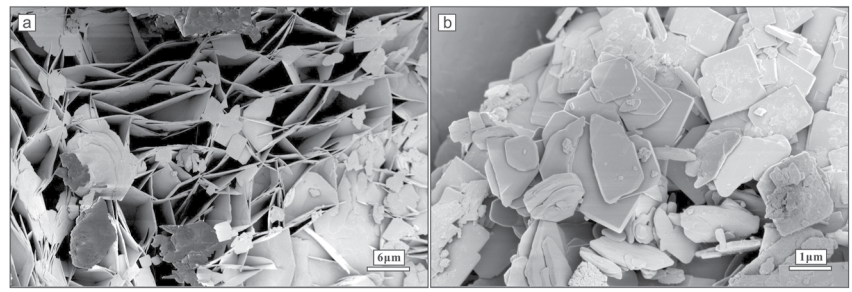

Figure 3. Representative scanning electron micrographs showing interlocking platy hydromagnesite crystals, which are typical of abiotic formation.

catchments respectively, significance confirmed by *t*-test-*P* values < 0.001). All these stream water Mg/Ca ratios are lower than alkaline lakes (mean of 14.5, n = 150, data sources in Table S5 in Supporting Information S2, Figure 4). Currently, input and DL waters are undersaturated with respect to hydromagnesite.

Stream and groundwater δ^{26}Mg values range from −0.53‰ to −1.46‰ (Table S2 in Supporting Information S2, Figure 4c), typical of river and groundwaters (Tipper et al., 2006a). Similar to the Mg/Ca ratio, the δ^{26}Mg values of lake waters are higher than input waters, ranging from −0.07‰ to +0.46‰ (mean = −0.16‰, Figure 4). ^{26}Mg enrichment is observed in other alkaline lakes and playas, compared to their input waters (Mavromatis et al., 2021; Shirokova et al., 2013; P. Zhang et al., 2021).

Both modern lake water and Holocene hydromagnesite ^{87}Sr/^{86}Sr ratios (which presumably provides a record of the aqueous ^{87}Sr/^{86}Sr ratio at the time of formation) are within the range of modern inputs (Figure 4b, Table S2 in Supporting Information S2). However, the ^{87}Sr/^{86}Sr ratios of modern lake water range from 0.708873 to 0.709353, similar to the minimum of measured input waters (0.708964 to 0.710363). The ^{87}Sr/^{86}Sr ratios of Holocene hydromagnesite ranged from 0.710045 to 0.710057, and is distinct from the modern lake. Typical uncertainties for ^{87}Sr/^{86}Sr ratios are smaller than 0.000008.

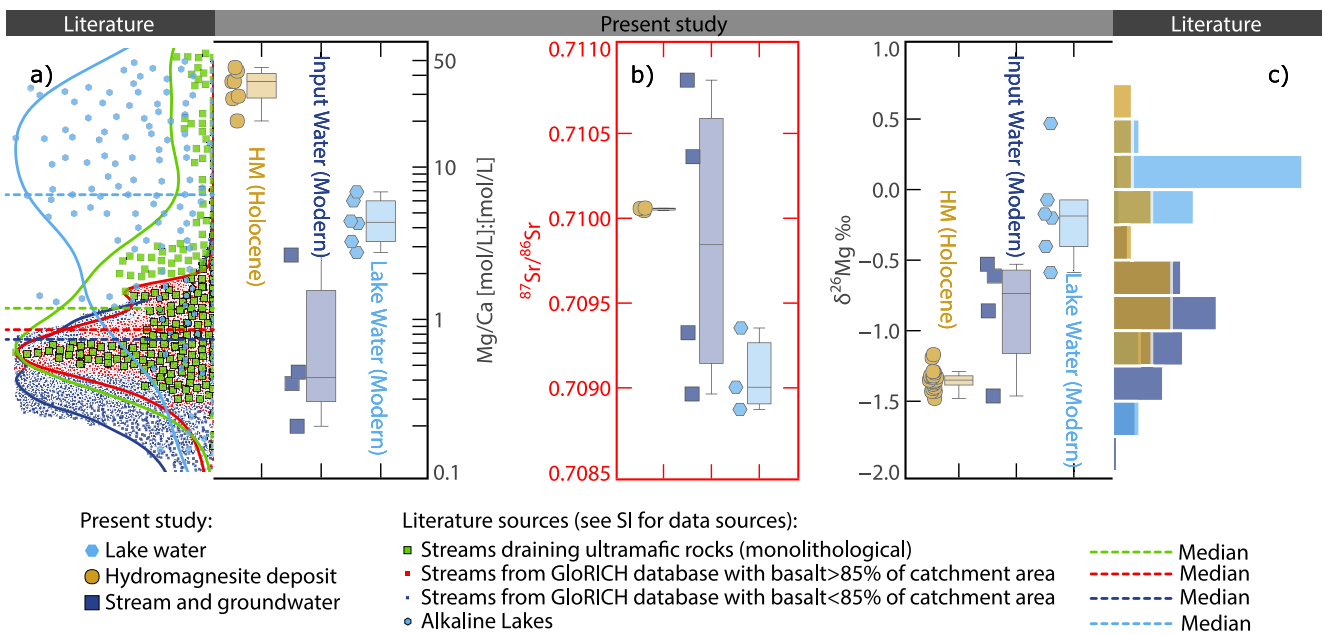

Figure 4. Dujiali Lake, input waters, and hydromagnesite compositions: (a) Mg/Ca ratios. Marginal density plots show (1) the GloRICH rivers database (Hartmann et al., 2014) filtered by catchments with <85% basalt in the catchment area, and <15% basalt, (2) small rivers draining only ultramafic rocks (Table S4 in Supporting Information S2), and (3) alkaline lake waters (Table S5 in Supporting Information S2). Dashed lines are the medians of each distribution. (b) Sr isotope ratios, (c) δ^{26}Mg ratios. The marginal histogram shows a literature compilation of river waters, lakes and playas, and lake waters and hydromagnesite δ^{26}Mg values (data source in Table S6 in Supporting Information S2).

5. Discussion

5.1. Abiotic Origins of Authigenic Hydromagnesite

The occurrence of hydromagnesite in alkaline lakes around the world is commonly (but not exclusively) associated with microbial mats and stromatolites (Braithwaite & Zedef, 1996; Gérard et al., 2013; Power et al., 2009; Renaut & Long, 1989; Sanz-Montero et al., 2019), or is stratabound (Goto et al., 2003; Jiang et al., 2021; Lin et al., 2017). Although microbes are known to mediate hydromagnesite formation under alkaline conditions, the exact role of microorganisms is poorly understood (Sanz-Montero et al., 2019). Laboratory experiments with cyanobacteria, using natural lake waters where hydromagnesite precipitates in the modern system (e.g., Bangkog Co, Tibet, and Atlin playa, Canada) precipitated dypingite ($Mg_5(CO_3)_4(OH)_2 \cdot 5H_2O$) rather than hydromagnesite (Jiang et al., 2021; Power et al., 2007). Power et al. (2007) suggested that the biologically mediated formation of dypingite could likely be a precursor for the formation of hydromagnesite via dehydration. However, dypingite cannot transform to hydromagnesite at a temperature lower than 100°C (Yamamoto et al., 2022). This transformation seems unlikely in the cold and arid QTP. Inorganic laboratory experiments have successfully precipitated hydromagnesite under various physical-chemical conditions (Berninger et al., 2014; Gautier et al., 2014), demonstrating that hydromagnesite can form in the absence of microbial activity.

SEM imaging of hydromagnesite crystals from DL demonstrates a plate-like morphology suggestive of an inorganic precipitation pathway (Power et al., 2019), with no conclusive evidence of microbes (Figure 3). Hydromagnesite precipitation associated with microbial mats typically forms radiating aggregates of hydromagnesite crystals because of the progressive deposition of plate-like crystals of hydromagnesite on the bacterial cells, which entomb the bacteria (Sanz-Montero et al., 2019). Finally, the $\delta^{13}C_{V\text{-}PDB}$ and $\delta^{18}O_{V\text{-}PDB}$ values of hydromagnesite in DL are positive, ranging from +5.3‰ to +6.5‰ and +4.1‰ to +5.2‰ respectively (Lin et al., 2017). This indicates (a) that microbial activity is minor and (b) that authigenic carbonate crystallizing from evaporated water is the dominant precipitation process in an evaporitic and abiotic environment.

5.2. Sr Isotope Constraints on Sources of Water Past and Present

The representability of the sampled stream and groundwaters for supplying solutes to the lake can be assessed with Sr isotopes (Lin et al., 2019a; Figure 4b). Streams and groundwaters have a considerable range in $^{87}Sr/^{86}Sr$ ratios between 0.709 and 0.711 (Table S2 in Supporting Information S2). The modern lake water $^{87}Sr/^{86}Sr$ ratios show a significant but narrower range (0.7089–0.7094), that is between the range of the modern inputs (within uncertainty). Although the lake water $^{87}Sr/^{86}Sr$ ratios fall within the range of modern inputs, they are at the low end of the modern inputs. This suggests that the two samples with the lower $^{87}Sr/^{86}Sr$ ratios are more representative of the modern inputs to the lake than the two samples with the higher $^{87}Sr/^{86}Sr$ ratios. In addition, the $^{87}Sr/^{86}Sr$ ratios of the bulk sediment are very different to the modern lake waters, streams, and hydromagnesite, suggesting an external detrital source and it is probable that clays, chlorite, quartz, and feldspar are supplied by streams or wind-blown dust. The $^{87}Sr/^{86}Sr$ ratios of Holocene hydromagnesite are distinct from the modern lake, indicating a change in hydrological regime since the Holocene.

The $^{87}Sr/^{86}Sr$ ratios of the Holocene hydromagnesite samples exhibit a narrow range from 0.71005 to 0.71006. This is higher than the modern lake waters, but within the range of the modern input waters, suggesting that at the time of hydromagnesite deposition, the input waters with higher $^{87}Sr/^{86}Sr$ ratios provided a more significant source of Sr compared to the modern system. Indeed, the stream water with the second highest $^{87}Sr/^{86}Sr$ ratio sample has the highest Mg/Ca ratio (DJS03), suggesting that the discharge-weighted Mg/Ca ratio in the past might have been higher than the present day. Although the input waters may have varied in composition within the range provided by modern $^{87}Sr/^{86}Sr$ ratios, given that all the input waters have lower $\delta^{26}Mg$ values and Mg/Ca ratios compared with the modern lake, we argue that it is unlikely that the source composition of the input waters could have varied to the extent that $\delta^{26}Mg$ values and Mg/Ca ratios are equal to those in the modern lake. Furthermore, it is likely that at the time of hydromagnesite formation, the Mg/Ca ratio of the lake water would have been even greater than that of the present day, making the difference in $\delta^{26}Mg$ values and Mg/Ca ratios between the lake and input waters even greater. Therefore, we argue that the difference in $\delta^{26}Mg$ values and Mg/Ca ratios between the stream waters and the lake is sustained by a fractionation associated with low-Mg carbonate (e.g., aragonite and/or low-Mg calcite) formation. Whilst the lake water $\delta^{26}Mg$ could be enriched in

^{26}Mg by both hydromagnesite and/or low-Mg carbonate formation and/or Mg clay formation, the Mg/Ca ratio of the lake waters can only be increased by low-Mg carbonate formation.

Differences between the chemistry of DL and river waters must either be caused by additional inputs of water to the lake, with extreme Mg/Ca ratios that weren't sampled, or a process that fractionates both Mg/Ca and $\delta^{26}Mg$ values. Ca is likely to be preferentially removed relative to Mg via elevating the Mg/Ca ratio of the lake water. This mechanism is important in aquifers and seawater (Smalley et al., 1994) and some alkaline lakes (Chagas et al., 2016; Zeyen et al., 2021). Minor calcite and dolomite were observed in the modern lake sediments. Dolomite was only observed in one of three lake sediments that were collected from a small depression on the edge of the lake that was likely isolated from the lake in the past, suggesting the dolomite has not precipitated from the present-day lake. Dolomite is rare in alkaline lakes and playa containing hydromagnesite deposits (Chagas et al., 2016; Zeyen et al., 2021), and its precipitation is kinetically inhibited at Earth surface temperatures and pressures and may not even occur when supersaturated in solution (Al Disi et al., 2021). Although dolomite could explain the Mg isotope offset between the input water and the lake, it is not considered further in the model that is developed below since it is not thought to form from the modern lake water. Calcite precipitation is typically inhibited at high Mg/Ca ratios (De Choudens-Sanchez & Gonzalez, 2009), and is not observed to precipitate contemporaneously with the hydromagnesite, and is also not considered in the model.

5.3. A Semi-Quantitative 1D Box Model

To evaluate whether low-Mg carbonate may elevate the Mg/Ca and Mg isotope ratio of the lake water, a semi-quantitative 1D box model was developed. An elemental flux from the ground and river waters supply the lake $\left(J^i_{in}\right)$ for chemical species i, for example, Ca^{2+}, Mg^{2+}, HCO_3^-. The elemental flux from the lake $\left(J^i_{\text{out}}\right)$ consists of carbonate sedimentation (aragonite, or hydromagnesite; both detected in the hydromagnesite deposit) or clay (present in modern sediments). The temporal variation of solutes in the lake $\left(N^i_{\text{Lake}}\right)$ is given by:

$$\frac{d\left(N^i_{\text{Lake}}\right)}{dt} = \sum\left(J^i_{in} - J^i_{\text{out}}\right) \tag{2}$$

For carbonate output:

$$Ca^{2+} + 2HCO_3^- \Rightarrow CaCO_3 + CO_2 + H_2O \tag{3}$$

$$5Mg^{2+} + 4CO_3^{2-} + 2OH^- + 4H_2O \Rightarrow Mg_5(CO_3)_4(OH)_2 \cdot 4H_2O \tag{4}$$

J^{Ca}_{out} and $J^{\text{Mg}}_{\text{out}}$ are linked via a partition coefficient (K_d) for Mg in aragonite via the equation:

$$\frac{J^{\text{Mg}}_{\text{out}}}{J^{\text{Ca}}_{\text{Out}}} = K_d \times (\text{Mg/Ca})_{\text{lake}} \tag{5}$$

The chemical equilibrium between the output mineral phases and lake water at each time-step provides a negative feedback, preventing runaway fractionation of Mg/Ca ratios (or $\delta^{26}Mg$ values) forcing the model to a steady state.

The $\delta^{26}Mg$ of the lake water and mineral output was determined using the equation:

$$\frac{d\left(N_{\text{Mg}} \cdot \delta^{26}\text{Mg}_{\text{lake}}\right)}{dt} = \sum\left(J^{\text{Mg}}_{in} \cdot \delta_{in} - J^{\text{Mg}}_{\text{out}} \cdot \delta_{\text{out}}\right) \tag{6}$$

where δ refers to $\delta^{26}Mg$. δ_{out} is related to the isotopic composition of the lake, $\delta^{26}Mg$, by the fractionation factor Δ:

$$\delta_{\text{out}} = \Delta \cdot \delta^{26}\text{Mg}_{\text{lake}} \tag{7}$$

where Δ refers to the fractionation factor between aqueous Mg and either aragonite, hydromagnesite, or clay.

5.3.1. Model Inputs to the Lake

The inputs to the lake were assumed to have the mean of the chemical composition of modern the river and groundwaters (Table S8 in Supporting Information S2). pCO_2 of the lake water was set to be in equilibrium with

pre-industrial atmospheric levels (280 ppm). Sensitivity testing pCO_2 (from pre-industrial to modern CO_2 concentrations) demonstrated insignificant changes in lake water pH with fixed chemical parameters.

The input discharge was estimated from the Cl^- concentration of the lake and the average river water, assuming that Cl^- is a conservative element, with no output from the lake since it was last dry and by estimating the residence time (τ) of Cl^- from the residence time equation (Richter et al., 1992):

$$\tau = N_{\text{Lake}}^{Cl-} / N_{in}^{Cl-} \tag{8}$$

where τ is the residence time, N_{Lake}^{Cl-} is the mass of Cl^- in the lake, and J_{in}^{Cl-} is the flux of Cl^- to the lake (product of discharge and concentration). The total mass of Cl^- in the lake is given by the product of the lake volume (estimated at $2.4e^8 m^3$ assuming an average water depth of 3 m) and mean Cl^-concentration of 22,547 μmol/L (Table S6 in Supporting Information S2). Given that the lake was dry in the 1980s, a residence time was estimated at between 20 and 40 years. This implies a range in the discharge of 5–10 cumecs and a typical discharge was therefore estimated as 7 cumecs. This discharge implies that there must either be a continual increase in water volume, or that there must be a significant level of evaporation. For example, to maintain constant water volume, an evaporation factor (defined as the annual loss of water from the lake) of 2 would be required to maintain a constant volume. Loss of water via evaporation and/or freezing was considered by evaluating the model over a range of evaporation factors from 2 to 4, concentrating the solutes of the lake waters and scaling the input fluxes by reducing the discharge by the evaporation factor.

5.3.2. Model Outputs From the Lake

The output from the lake was determined assuming the lake water was at equilibrium with aragonite, hydromagnesite, and/or sepiolite ($Mg_4Si_6O_{15}(OH)_2 \cdot 6H_2O$), an Mg-rich clay of the smectite group found in lake sediments (Mulders & Oelkers, 2020), used as a control for clay mineral formation. Sepiolite does not contain iron or aluminum; these two components are not readily available in the lake water, making it a good candidate for Mg removal via clay. These three phases were chosen on the basis that aragonite and hydromagnesite are observed to co-exist in the hydromagnesite deposit. The model does not account for dolomite formation as discussed above. At each time-step of the box model, phase equilibria were calculated using PHREEQC (Parkhurst & Appelo, 2013) at 1°C, assuming that the equilibrium phases aragonite, hydromagnesite, and sepiolite could precipitate provided that saturation state conditions were met. All phase equilibria were calculated in PHREEQC implemented in R (version 4.1.1) using the phreeqc and tidyphreeqc (https://github.com/paleolimbot/tidyphreeqc.git) libraries. The ThermoddemV1.10 (Blanc et al., 2012) was used for all calculations. For aragonite the saturation index (SI) for precipitation was assumed to be 0, for sepiolite, the SI was assumed to be 1, and for hydromagnesite, the influence of different SI between 1 and 5 was investigated, equivalent to considering a range of kinetic overstep for nucleation and growth. It is noted that although the calculations were made at 1°C, the thermodynamic data in the database were determined at higher temperatures and was extrapolated to 1°C.

5.3.3. Additional Model Variables and Model Implementation

The model accounts for the sources and sinks of the species Ca^{2+}, Mg^{2+}, Si, and HCO_3^-, through the supply via streams and sink via aragonite, hydromagnesite, and sepiolite. There is no sink in the model for the elements Na^+, K^+, Cl^-, and SO_4^{2-} and these elements accumulate in the lake progressively, increasing the salinity.

Model solutions were investigated for a K_d between 0.001 and 0.005. This range is high (Mavromatis et al., 2022) testing the maximum sensitivity of the model to the incorporation of Mg in aragonite. The fractionation factor for hydromagnesite was evaluated as a variable, between 0‰ and −1‰ (Mavromatis et al., 2021; Oelkers et al., 2018; Shirokova et al., 2013). The fractionation factor for aragonite was also evaluated as a variable, between 0‰ and −2‰ (Son et al., 2020; Wang et al., 2013; Wombacher et al., 2011). The fractionation factors associated with clay minerals are poorly known (Hindshaw et al., 2020; Voigt et al., 2020), but are generally <1‰ in magnitude. To evaluate the sensitivity of $\delta^{26}Mg_{\text{Hydromagnesite}}$ and $\delta^{26}Mg_{\text{Lake}}$ to the impact of the incorporation of Mg into clays, a fractionation factor of 1‰ for sepiolite was assumed, and model output compared with and without sepiolite formation.

Equations 2 and 6 were evaluated by finite difference with a time-step of 0.05 years. The calculated amount of aragonite, hydromagnesite, and sepiolite was converted to the molar output from the lake at each time step, and a new lake composition was determined, taking into account the mineral stoichiometry. The model does not assume

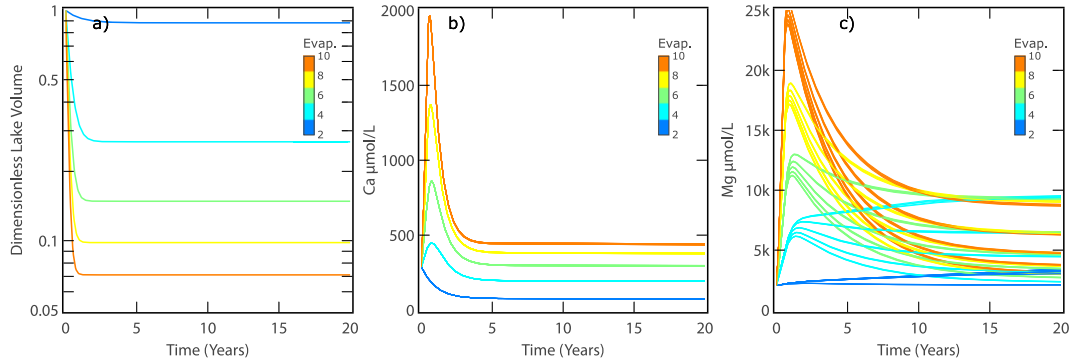

Figure 5. The variation of dimensionless lake volume, Ca and Mg concentration colored by the degree of evaporation.

a steady state, but because the output from the lake is a function of the lake chemistry, the lake chemistry acts as feedback on the lake output, meaning that the model will self-adjust to a steady state for most sets of input parameters. A "control" model was also run, with no precipitation of sepiolite, to enable a comparison of δ^{26}Mg values with and without clay formation in the lake. For both "control" and default models, a total of 3,750 different permutations of parameter space were evaluated.

5.4. Model Results

5.4.1. Water Balance and Chemical Concentrations

Changing the degree of evaporation changes the steady-state volume of water in the lake (Figure 5). Evidently, the volume of water in the lake has not remained at a steady state since the lake was dry in the 1980s. Drying of the lake increases the concentrations of solutes in the lake. The increase in solutes, in turn, increases the saturation states of minerals (aragonite, hydromagnesite, and sepiolite), causing precipitation which then decreases the concentration of solutes in the lake until a steady state is reached. The modeled Mg concentrations have an additional level of complexity in the model, because of the parameterization of the SI of hydromagnesite $\left(SI_{Hydromagnesite}\right)$ precipitation between 1 and 5. Whilst evaporation is the dominant control on Mg concentrations, the dispersion at each level of evaporation on Figure 5c is caused by changing the SI index for hydromagnesite precipitation between 1 and 5.

5.4.2. Mineral and Mg Output From the Lake

The highest modal fraction of hydromagnesite predicted by the model was 86% (Figure 6), approximately 10% lower than the observed value. Out of the 3,750 modal runs over different combinations of input parameter space ($Kd_{Aragonite}$, evaporation, $SI_{hydromagnesite}$, $\Delta_{Aragonite}$, and $\Delta_{Hydromagnesite}$), 600 reached modal hydromagnesite >85%.

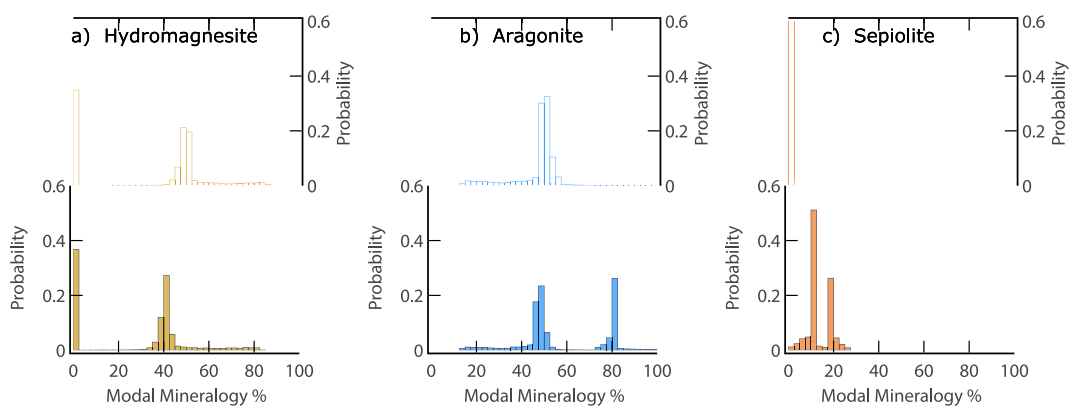

Figure 6. Histograms of modal mineralogy of model output, where each count corresponds to one of the 3,750 different combinations of parameter space investigated. Upper plots are the control model, where no Mg clay (sepiolite) was permitted to precipitate.

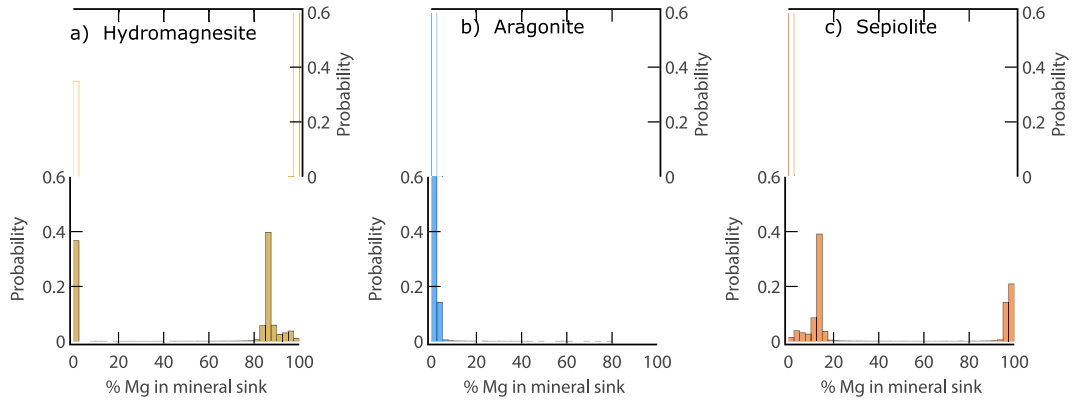

Figure 7. Histograms of Mg output from the lake by the mineral of model output, where each count corresponds to one of the 3,750 different combinations of parameter space investigated. Upper plots are the control model, where no Mg clay (sepiolite) was permitted to precipitate.

This is close to the observed modal mineralogy of the hydromagnesite deposit with >95% hydromagnesite and <5% aragonite. This maximum modal value of hydromagnesite was the same, regardless of whether or not clay was permitted to precipitate, although the total modal proportions of hydromagnesite are lower (Figure 6). This, combined with the lack of clay observed in the hydromagnesite, makes clay formation during the deposition of the hydromagnesite unlikely. When the clay was included in the model, the maximum modal fraction of clay at any individual time step was <30% (Figure 6c). This is lower than the observed clay fraction in the modern lake sediments, but it is noted that a given proportion of these clays are probably detrital in origin.

Since the Mg content of aragonite is small (as constrained by the partition coefficient) the percentage of Mg in aragonite is only ever appreciable when neither hydromagnesite nor sepiolite precipitate (Figure 7). The percentage of Mg in sepiolite only ever exceeds 20% in the model scenarios where hydromagnesite does not precipitate. In contrast, the majority of the model runs have a percentage of Mg in hydromagnesite in excess of 80% (Figure 7).

5.4.3. Lake Mg/Ca Ratios and Hydromagnesite Formation

The model results show that aragonite precipitation increases the Mg/Ca ratios of the lake over time to a maximum value of ~56 (Figure 8, Figure S2 in Supporting Information S1). The time of the Mg/Ca peak depends on the input flux, relative to the mass of solutes in the lake. The onset of hydromagnesite precipitation reduces the Mg/Ca to a steady state value close to the input value. The model predicts a wide envelope of Mg/Ca ratios, mostly dependent on (a) the degree of evaporation/freezing of the lake water (Table S9 in Supporting Information S2) which elevates concentrations of chemical species compensating removal via mineral output, and (b) the SI at which hydromagnesite precipitates. Whilst there is a wide range of Mg/Ca ratios across the entirety of parameter space, a restricted range of solutions (dark shading on Figure 8a) match the observed modal mineralogy with hydromagnesite ~85% (contour lines on Figure 8a) for a transient period.

These model solutions are insensitive to K_d (Aragonite) but they are strongly dependent on $SI_{hydromagnesite}$ and evaporation with modal hydromagnesite >85% requiring $SI_{hydromagnesite}$ <2 and a degree of evaporation >3.5. $SI_{hydromagnesite}$ is qualitatively related to the energy overstep that is required to nucleate hydromagnesite, suggesting that the degree of supersaturation might be relatively low for the spontaneous nucleation of hydromagnesite in these natural conditions.

A key feature of hydromagnesite deposits in alkaline lakes (and playas) is the mixture of hydromagnesite and aragonite (Braithwaite & Zedef, 1996; Goto et al., 2003; Power et al., 2009). The model predicts continuous stratigraphy where the proportion of hydromagnesite to aragonite increases in DL reaching a peak greater than 85% (Figure S4 in Supporting Information S1), close to the observed 95% in bulk hydromagnesite, before decreasing. This would predict an alternating sequence of aragonite-rich layers, followed by hydromagnesite-rich layers in the lake. There is no core material at DL. However, a core from nearby Selin Co Lake (Figure 1) shows alternating stratigraphy between Holocene hydromagnesite and low-Mg carbonate (Goto et al., 2003), supportive of the model concept.

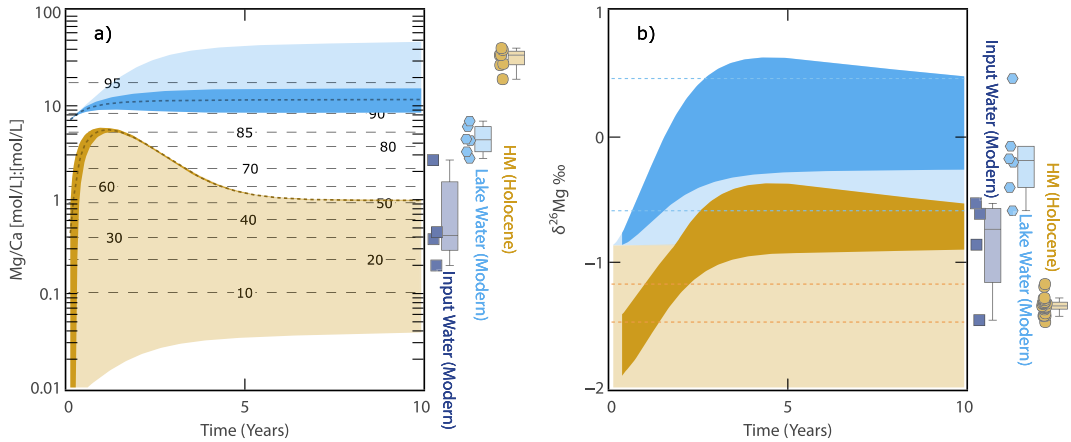

Figure 8. Example model output as a function of time. (a) Mg/Ca ratio in lake water (blue) and hydromagnesite (brown). Horizontal contours are modal mineralogy (aragonite/hydromagnesite). Dark shading indicates the model results that fit best with the observed high fraction of hydromagnesite relative to aragonite. (b) δ^{26}Mg values in lake water (blue) and hydromagnesite (brown). Dark shading indicates the range of model solutions consistent with both the modal mineralogy and the δ^{26}Mg. Horizontal dotted lines indicate the range of the modern lake water (blue) and Holocene hydromagnesite (brown). The marginal box-plot shows the measured data. The dark shaded area is where model output reaches >85% Aragonite. The pale area is all model output.

5.5. Mg Isotope Constraints on the Evaporative Environments for Hydromagnesite Formation

Mg-rich clays, such as sepiolite, could have a major influence on the δ^{26} Mg value of the lake. The sensitivity of the model to clay formation as an authigenic phase was tested by allowing clay (sepiolite) to precipitate at a SI of 1, and compared to a control scenario, where clay formation was negligible, by setting the SI of sepiolite to 50. The δ^{26}Mg values of the bulk carbonate output for all model runs are compared in Figure 9. The model output is relatively insensitive to Mg output via clay, with the difference in δ^{26}Mg values between the control model (no clay) with the model run with clay output <0.25‰ (Figure 9), largely because the model estimates the Mg output via clay to be modest, <20% of the total Mg output.

δ^{26}Mg values of both the hydromagnesite deposit (mixture of hydromagnesite and aragonite) are controlled by both the Mg isotope fractionation factors associated with each of the mineral sinks of Mg, in addition to the fraction of Mg in each mineral (Figure 7), with each mole of hydromagnesite and sepiolite containing 5 and 4 mol of Mg respectively. Since the Mg content of the aragonite is very small, aragonite could only ever have leverage on the δ^{26}Mg value of the lake water (and by implication the hydromagnesite) if the fractionation factor was significantly lower than the minimum value of −2‰ that was evaluated by the model.

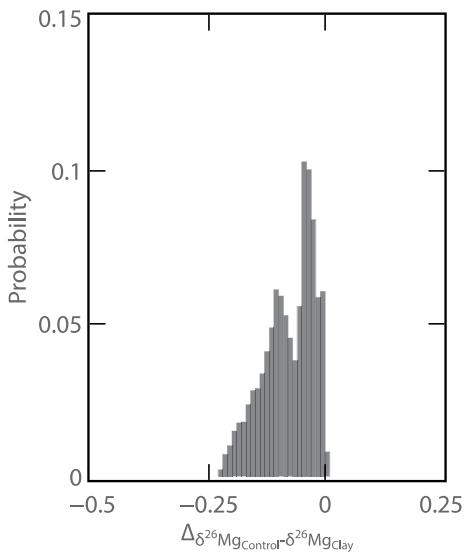

Figure 9. The difference in δ^{26}Mg values of bulk carbonate between the control model (no clay) and the model output with clay and all time-steps.

Of the model solutions that predict modal hydromagnesite >85%, even fewer (275 out of 3,750) converged to the observed range of δ^{26}Mg values in the hydromagnesite deposit (dark shaded area on Figure 8, Figure S3 in Supporting Information S1). These model solutions impose the constraint that $SI_{hydromagnesite} < 2$ and a degree of evaporation >3.5, and $\Delta_{hydromagnesite}$ <−0.6‰, a reasonable estimate compared to literature values (Mavromatis et al., 2021; Oelkers et al., 2018; Shirokova et al., 2013). The high evaporation is consistent with carbon and oxygen isotope data from the hydromagnesite deposit (Lin et al., 2017), and their positive values are associated with evaporative and restricted environments.

5.6. Implication for the Mechanisms of Hydromagnesite Precipitation

The majority of documented occurrences of hydromagnesite are distributed in proximity to alkaline lakes and playas in the vicinity of ultramafic rocks

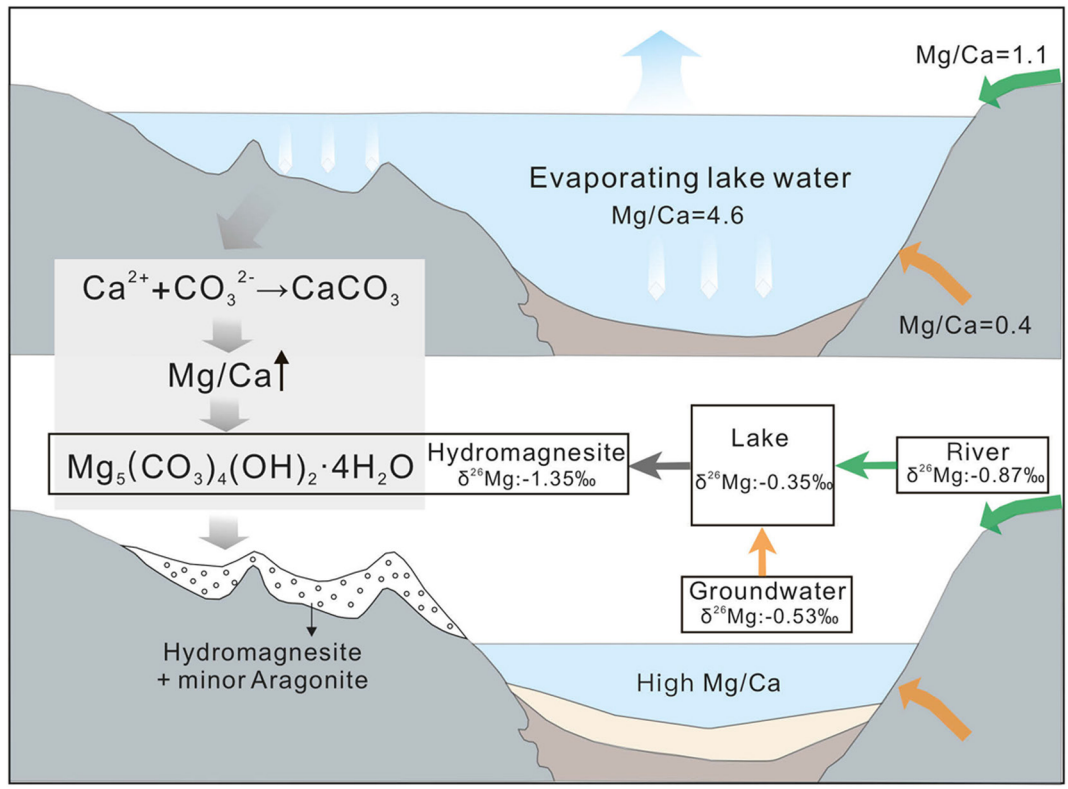

Figure 10. Conceptual model of hydromagnesite formation process in Dujiali Lake.

(Braithwaite & Zedef, 1996; Power et al., 2009). In general, the origin of Mg-bearing solutions forming sedimentary hydromagnesite in alkaline lakes and playas is commonly associated with the weathering of ultramafic rocks (Braithwaite & Zedef, 1996; Power et al., 2009). However, the Mg/Ca ratios of water draining ultramafic rocks is not always high enough for hydromagnesite formation (Last et al., 2010). These stream water Mg/Ca ratios are lower than alkaline lakes (mean of 14.5, n = 150, Figure 4, data sources in Table S5 in Supporting Information S2) and much lower than that required for the precipitation of hydromagnesite (Chagas et al., 2016). The chemical weathering of ultramafic rocks provides an important source of Mg to these alkaline lakes and playas but the Mg/Ca ratios of these input waters in most settings are seldom high enough for hydromagnesite precipitation (Last et al., 2010). Therefore, it is likely that the removal of Ca^{2+} from lake waters from low Mg carbonate precipitation (e.g., calcite and aragonite) occurred prior to hydromagnesite formation.

The modes for hydromagnesite formation in alkaline lakes such as Dujiali, demonstrate a period of time where the combination of hydrology and climatic conditions were conducive to large-scale hydromagnesite precipitation that is distinct from the modern environment. Significant lake expansion has occurred in QTP in recent decades (Liu et al., 2021), including DL, due to the increase of precipitation and meltwater from ice, which might be the reason why hydromagnesite precipitated during the Holocene but not at the present day. In this study, we simulated the behavior of the carbonate system during the hydrochemical evolution of lake chemistry under evaporation scenarios. As discussed above, intense evaporation, high alkalinity, and high Mg/Ca ratios are important environmental factors in favor of hydromagnesite precipitation. In this setting, evaporation contributes to increased salinity and alkalinity of lake waters, driving aragonite precipitation which in turn increased Mg/Ca ratios. The high Mg/Ca ratios and alkalinity are key drivers of hydromagnesite formation in the majority of alkaline lakes and playas (Figure 10), which was supported by the common field observation from alkaline lakes and playas that hydromagnesite and aragonite co-exist (Braithwaite & Zedef, 1996; Goto et al., 2003; Power et al., 2009; Zeyen et al., 2021).

6. Conclusion

The presence of hydromagnesite in alkaline lakes requires high Mg/Ca ratios, and was previously mainly attributed to the weathering of ultramafic lithologies. At DL, ultramafic rocks are extensive, but presently the Mg/Ca

ratios of input waters are much lower than that required for hydromagnesite precipitation. Differences between the chemistry of alkaline lakes and recharge waters are most likely caused by a process which fractionates Mg/Ca ratios and δ^{26}Mg values. A semi-quantitative box model of the lake chemistry was developed using Phreeqc to investigate the behavior of the carbonate system and Mg isotopes during the evolution of the lake chemistry. Here, we suggest an alternative/additional control on hydromagnesite formation in alkaline lakes is low-Mg carbonate (aragonite) precipitation under evaporative conditions. We note that at a global scale rivers, groundwater, and lakes do not typically have Mg/Ca ratios great enough to precipitate hydromagnesite. Although the ultramafic Mg source rocks are important for hydromagnesite precipitation, the influence of an essential precursor that removes Ca in a greater proportion than Mg is required for spontaneous hydromagnesite precipitation. This study provides an improved understanding of the modes of sediment deposition and environmental conditions at the time of hydromagnesite deposition, which may be a natural analog for some strategies of CO_2 mineral carbonation.

Data Availability Statement

All data used in this study are stored on Zenodo (https://zenodo.org/record/6981702#.YvUwNOzMLfA). All phase equilibria were calculated in PHREEQC (Parkhurst & Appelo, 2013) implemented in R (version 4.1.1) using the phreeqc and tidyphreeqc libraries (https://github.com/paleolimbot/tidyphreeqc.git). The ThermoddemV1.10 (Blanc et al., 2012) was used for all calculations.

Acknowledgments
The authors thank Emily Stevenson, Luke Bridgestock, Alasdair Knight, Linshu Feng, and Nicholas Tosca for helpful discussions and suggestions. In a previous form, this manuscript benefitted from extensive comments from Eric Oelkers and three anonymous reviewers. This research was supported by the National Natural Science Foundation of China (42102115), the Second Tibetan Plateau Scientific Expedition and Research Program (2022QZKK0201), and the Observation and Research Station of Salt Lakes in Tibetan Plateau. YL acknowledges funding from the China Scholarship Council. ETT acknowledges the NERC funding NE/T007214/1, NE/P011659/1, and NE/M001865/1, and WJK NERC studentship NE/S007164/1.

References

Al Disi, Z. A., Zouari, N., Attia, E., Al-Asali, M., Al-Kuwari, H. A. S., Sadooni, F., et al. (2021). Systematic laboratory approach to produce Mg-rich carbonates at low temperature. *RSC Advances*, *11*(59), 37029–37039. https://doi.org/10.1039/d1ra06206a

Allegre, C. J., Poirier, J.-P., Humler, E., & Hofmann, A. W. (1995). The chemical composition of the Earth. *Earth and Planetary Science Letters*, *134*(3–4), 515–526. https://doi.org/10.1016/0012-821x(95)00123-t

Berninger, U. N., Jordan, G., Schott, J., & Oelkers, E. H. (2014). The experimental determination of hydromagnesite precipitation rates at 22.5–75°C. *Mineralogical Magazine*, *78*(6), 1405–1416. https://doi.org/10.1180/minmag.2014.078.6.07

Blanc, P., Lassin, A., Piantone, P., Azaroual, M., Jacquemet, N., Fabbri, A., & Gaucher, E. C. (2012). Thermoddem: A geochemical database focused on low temperature water/rock interactions and waste materials. *Applied Geochemistry*, *27*(10), 2107–2116. https://doi.org/10.1016/j.apgeochem.2012.06.002

Braithwaite, C., & Zedef, V. (1996). Hydromagnesite stromatolites and sediments in an alkaline lake, Salda Golu, Turkey. *Journal of Sedimentary Research*, *66*(5), 991–1002.

Broughton, P. L. (1972). Monohydrocalcite in speleothems: An alternative interpretation. *Contributions to Mineralogy and Petrology*, *36*(2), 171–174. https://doi.org/10.1007/bf00371187

Canaveras, J. C., Hoyos, M., Sanchez-Moral, S., Sanz-Rubio, E., Bedoya, J., Soler, V., et al. (1999). Microbial communities associated with hydromagnesite and needle-fiber aragonite deposits in a karstic cave (Altamira, Northern Spain). *Geomicrobiology Journal*, *16*(1), 9–25. https://doi.org/10.1080/014904599270712

Chagas, A. A., Webb, G. E., Burne, R. V., & Southam, G. (2016). Modern lacustrine microbialites: Towards a synthesis of aqueous and carbonate geochemistry and mineralogy. *Earth-Science Reviews*, *162*, 338–363. https://doi.org/10.1016/j.earscirev.2016.09.012

De Choudens-Sanchez, V., & Gonzalez, L. A. (2009). Calcite and aragonite precipitation under controlled instantaneous supersaturation: Elucidating the role of $CaCO_3$ saturation state and Mg/Ca ratio on calcium carbonate polymorphism. *Journal of Sedimentary Research*, *79*(6), 363–376. https://doi.org/10.2110/jsr.2009.043

Fischbeck, R., & Müller, G. (1971). Monohydrocalcite, hydromagnesite, nesquehonite, dolomite, aragonite, and calcite in speleothems of the Fränkische Schweiz, Western Germany. *Contributions to Mineralogy and Petrology*, *33*(2), 87–92. https://doi.org/10.1007/bf00386107

Fukushi, K., & Matsumiya, H. (2018). Control of water chemistry in alkaline lakes: Solubility of monohydrocalcite and amorphous magnesium carbonate in $CaCl_2$–$MgCl_2$–Na_2CO_3 solutions. *ACS Earth and Space Chemistry*, *2*(7), 735–744. https://doi.org/10.1021/acsearthspacechem.8b00046

Gautier, Q., Bénézeth, P., Mavromatis, V., & Schott, J. (2014). Hydromagnesite solubility product and growth kinetics in aqueous solution from 25 to 75°C. *Geochimica et Cosmochimica Acta*, *138*, 1–20. https://doi.org/10.1016/j.gca.2014.03.044

Gérard, E., Ménez, B., Couradeau, E., Moreira, D., Benzerara, K., Tavera, R., & López-García, P. (2013). Specific carbonate–microbe interactions in the modern microbialites of Lake Alchichica (Mexico). *The ISME Journal*, *7*(10), 1997–2009. https://doi.org/10.1038/ismej.2013.81

Goto, A., Arakawa, H., Morinaga, H., & Sakiyama, T. (2003). The occurrence of hydromagnesite in bottom sediments from Lake Siling, central Tibet: Implications for the correlation among $\delta^{18}O$, $\delta^{13}C$ and particle density. *Journal of Asian Earth Sciences*, *21*(9), 979–988. https://doi.org/10.1016/s1367-9120(02)00169-4

Harrison, A. L., Bénézeth, P., Schott, J., Oelkers, E. H., & Mavromatis, V. (2021). Magnesium and carbon isotope fractionation during hydrated Mg-carbonate mineral phase transformations. *Geochimica et Cosmochimica Acta*, *293*, 507–524. https://doi.org/10.1016/j.gca.2020.10.028

Hartmann, J., Lauerwald, R., & Moosdorf, N. (2014). A brief overview of the GLobal River Chemistry Database, GLORICH. *Procedia Earth and Planetary Science*, *10*, 23–27. https://doi.org/10.1016/j.proeps.2014.08.005

Hindshaw, R. S., Tosca, R., Tosca, N. J., & Tipper, E. T. (2020). Experimental constraints on Mg isotope fractionation during clay formation: Implications for the global biogeochemical cycle of Mg. *Earth and Planetary Science Letters*, *531*, 115980. https://doi.org/10.1016/j.epsl.2019.115980

Horgan, B. H., Anderson, R. B., Dromart, G., Amador, E. S., & Rice, M. S. (2020). The mineral diversity of Jezero crater: Evidence for possible lacustrine carbonates on Mars. *Icarus*, *339*, 113526. https://doi.org/10.1016/j.icarus.2019.113526

Hu, Z., Hu, W., Wang, X., Lu, Y., Wang, L., Liao, Z., & Li, W. (2017). Resetting of Mg isotopes between calcite and dolomite during burial metamorphism: Outlook of Mg isotopes as geothermometer and seawater proxy. *Geochimica et Cosmochimica Acta*, *208*, 24–40. https://doi.org/10.1016/j.gca.2017.03.026

Jiang, T., Ji, L., Chen, H., Li, B., Li, G., Ma, H., et al. (2021). Algae mineralization experiment and genetic analysis of hydromagnesite in Bangor Lake, Xizang (Tibet). *Geological Review*, *67*(6), 1–19.

Königsberger, E., Königsberger, L. C., & Gamsjäger, H. (1999). Low-temperature thermodynamic model for the system Na_2CO_3–$MgCO_3$–$CaCO_3$–H_2O. *Geochimica et Cosmochimica Acta*, *63*(19–20), 3105–3119. https://doi.org/10.1016/s0016-7037(99)00238-0

Last, F. M., Last, W. M., & Halden, N. M. (2010). Carbonate microbialites and hardgrounds from Manito Lake, an alkaline, hypersaline lake in the northern Great Plains of Canada. *Sedimentary Geology*, *225*(1–2), 34–49. https://doi.org/10.1016/j.sedgeo.2010.01.006

Li, W., Beard, B. L., & Johnson, C. M. (2011). Exchange and fractionation of Mg isotopes between epsomite and saturated $MgSO_4$ solution. *Geochimica et Cosmochimica Acta*, *75*(7), 1814–1828. https://doi.org/10.1016/j.gca.2011.01.023

Li, W., Bialik, O. M., Wang, X., Yang, T., Hu, Z., Huang, Q., et al. (2019). Effects of early diagenesis on Mg isotopes in dolomite: The roles of Mn (IV)-reduction and recrystallization. *Geochimica et Cosmochimica Acta*, *250*, 1–17. https://doi.org/10.1016/j.gca.2019.01.029

Li, W., Chakraborty, S., Beard, B. L., Romanek, C. S., & Johnson, C. M. (2012). Magnesium isotope fractionation during precipitation of inorganic calcite under laboratory conditions. *Earth and Planetary Science Letters*, *333*, 304–316. https://doi.org/10.1016/j.epsl.2012.04.010

Lin, Y., Zheng, M., & Ye, C. (2017). Hydromagnesite precipitation in the alkaline Lake Dujiali, central Qinghai-Tibetan Plateau: Constraints on hydromagnesite precipitation from hydrochemistry and stable isotopes. *Applied Geochemistry*, *78*, 139–148. https://doi.org/10.1016/j.apgeochem.2016.12.020

Lin, Y., Zheng, M., Ye, C., & Power, I. M. (2019a). Rare Earth element and strontium isotope geochemistry in Dujiali Lake, central Qinghai-Tibet Plateau, China: Implications for the origin of hydromagnesite deposits. *Geochemistry*, *79*(2), 337–346. https://doi.org/10.1016/j.chemer.2019.02.002

Lin, Y., Zheng, M., Ye, C., & Power, I. M. (2019b). Trace and rare Earth element geochemistry of Holocene hydromagnesite from Dujiali Lake, central Qinghai–Tibetan Plateau, China. *Carbonates and Evaporites*, *34*(4), 1265–1279. https://doi.org/10.1007/s13146-017-0395-9

Liu, W., Xie, C., Zhao, L., Li, R., Liu, G., Wang, W., et al. (2021). Rapid expansion of lakes in the endorheic basin on the Qinghai-Tibet Plateau since 2000 and its potential drivers. *Catena*, *197*, 104942. https://doi.org/10.1016/j.catena.2020.104942

Mavromatis, V., Brazier, J.-M., & Goetschl, K. E. (2022). Controls of temperature and mineral growth rate on Mg incorporation in aragonite. *Geochimica et Cosmochimica Acta*, *317*, 53–64. https://doi.org/10.1016/j.gca.2021.10.015

Mavromatis, V., Power, I. M., Harrison, A., Beinlich, A., Dipple, G., & Bénézeth, P. (2021). Mechanisms controlling the Mg isotope composition of hydromagnesite-magnesite playas near Atlin, British Columbia, Canada. *Chemical Geology*, *579*, 120325. https://doi.org/10.1016/j.chemgeo.2021.120325

Mulders, J. J., & Oelkers, E. H. (2020). An experimental study of sepiolite dissolution rates and mechanisms at 25°C. *Geochimica et Cosmochimica Acta*, *270*, 296–312. https://doi.org/10.1016/j.gca.2019.11.026

Oelkers, E. H., Berninger, U.-N., Pérez-Fernàndez, A., Chmeleff, J., & Mavromatis, V. (2018). The temporal evolution of magnesium isotope fractionation during hydromagnesite dissolution, precipitation, and at equilibrium. *Geochimica et Cosmochimica Acta*, *226*, 36–49. https://doi.org/10.1016/j.gca.2017.11.004

Oskierski, H., Turvey, C. C., Wilson, S. A., Dlugogorski, B. Z., Altarawneh, M., & Mavromatis, V. (2021). Mineralisation of atmospheric CO_2 in hydromagnesite in ultramafic mine tailings–insights from Mg isotopes. *Geochimica et Cosmochimica Acta*, *309*, 191–208. https://doi.org/10.1016/j.gca.2021.06.020

Parkhurst, D. L., & Appelo, C. (2013). Description of input and examples for PHREEQC version 3—A computer program for speciation, batch-reaction, one-dimensional transport, and inverse geochemical calculations. *US Geological Survey Techniques And Methods*, *6*(A43), 497.

Power, I. M., Harrison, A. L., Dipple, G. M., Wilson, S. A., Barker, S. L., & Fallon, S. J. (2019). Magnesite formation in playa environments near Atlin, British Columbia, Canada. *Geochimica et Cosmochimica Acta*, *255*, 1–24. https://doi.org/10.1016/j.gca.2019.04.008

Power, I. M., Wilson, S. A., Harrison, A. L., Dipple, G. M., McCutcheon, J., Southam, G., & Kenward, P. A. (2014). A depositional model for hydromagnesite–magnesite playas near Atlin, British Columbia, Canada. *Sedimentology*, *61*(6), 1701–1733. https://doi.org/10.1111/sed.12124

Power, I. M., Wilson, S. A., Thom, J. M., Dipple, G. M., Gabites, J. E., & Southam, G. (2009). The hydromagnesite playas of Atlin, British Columbia, Canada: A biogeochemical model for CO_2 sequestration. *Chemical Geology*, *260*(3–4), 286–300. https://doi.org/10.1016/j.chemgeo.2009.01.012

Power, I. M., Wilson, S. A., Thom, J. M., Dipple, G. M., & Southam, G. (2007). Biologically induced mineralization of dypingite by cyanobacteria from an alkaline wetland near Atlin, British Columbia, Canada. *Geochemical Transactions*, *8*(1), 1–16. https://doi.org/10.1186/1467-4866-8-13

Qu, Y., Wang, Y., & Duan, J. (2011). *Geological survey reports of the regional People's Republic of China (scale 1:250000. duoba pieces)* (Chinese ed.). China University of Geosciences Press.

Renaut, R. W., & Long, P. R. (1989). Sedimentology of the saline lakes of the Cariboo Plateau, interior British Columbia, Canada. *Sedimentary Geology*, *64*(4), 239–264. https://doi.org/10.1016/0037-0738(89)90051-1

Richter, F. M., Rowley, D. B., & DePaolo, D. J. (1992). Sr isotope evolution of seawater: The role of tectonics. *Earth and Planetary Science Letters*, *109*(1–2), 11–23. https://doi.org/10.1016/0012-821x(92)90070-c

Saldi, G. D., Jordan, G., Schott, J., & Oelkers, E. H. (2009). Magnesite growth rates as a function of temperature and saturation state. *Geochimica et Cosmochimica Acta*, *73*(19), 5646–5657. https://doi.org/10.1016/j.gca.2009.06.035

Sanz-Montero, M. E., Cabestrero, Ó., & Sánchez-Román, M. (2019). Microbial Mg-rich carbonates in an extreme alkaline lake (Las Eras, central Spain). *Frontiers in Microbiology*, *10*, 148. https://doi.org/10.3389/fmicb.2019.00148

Scheller, E. L., Swindle, C., Grotzinger, J., Barnhart, H., Bhattacharjee, S., Ehlmann, B. L., et al. (2021). Formation of magnesium carbonates on Earth and implications for Mars. *Journal of Geophysical Research: Planets*, *126*(7), e2021JE006828. https://doi.org/10.1029/2021je006828

Shirokova, L. S., Mavromatis, V., Bundeleva, I. A., Pokrovsky, O. S., Bénézeth, P., Gérard, E., et al. (2013). Using Mg isotopes to trace cyanobacterially mediated magnesium carbonate precipitation in alkaline lakes. *Aquatic Geochemistry*, *19*(1), 1–24. https://doi.org/10.1007/s10498-012-9174-3

Smalley, P., Higgins, A., Howarth, R., Nicholson, H., Jones, C., Swinburne, N., & Bessa, J. (1994). Seawater Sr isotope variations through time: A procedure for constructing a reference curve to date and correlate marine sedimentary rocks. *Geology*, *22*(5), 431–434. https://doi.org/10.1130/0091-7613(1994)022<0431:ssivtt>2.3.co;2

Son, S., Li, W., Lee, J.-Y., & Kwon, K. D. (2020). On the coordination of Mg^{2+} in aragonite: Ab-initio absorption spectroscopy and isotope fractionation study. *Geochimica et Cosmochimica Acta*, *286*, 324–335. https://doi.org/10.1016/j.gca.2020.07.023

Sun, D., Li, B., Ma, Y., & Liu, Q. (2002). An investigation on evaporating experiments for Qinghai Lake water, China. *Journal of Salt Lake Research*, *10*(4), 1–12.

Tipper, E. T. (2022). *Magnesium isotopes: Tracer for the global biogeochemical cycle of magnesium past and present or archive of alteration*, Elements in Geochemical Tracers in Earth System Science. Cambridge University Press.

Tipper, E. T., Galy, A., & Bickle, M. J. (2008). Calcium and magnesium isotope systematics in rivers draining the Himalaya-Tibetan-Plateau region: Lithological or fractionation control? *Geochimica et Cosmochimica Acta*, *72*(4), 1057–1075. https://doi.org/10.1016/j.gca.2007.11.029

Tipper, E. T., Galy, A., Gaillardet, J., Bickle, M., Elderfield, H., & Carder, E. (2006a). The magnesium isotope budget of the modern ocean: Constraints from riverine magnesium isotope ratios. *Earth and Planetary Science Letters*, *250*(1–2), 241–253. https://doi.org/10.1016/j.epsl.2006.07.037

Tipper, E. T., Galy, A., Gaillardet, J., Bickle, M., Elderfield, H., & Carder, E. (2006b). The Mg isotope budget of the modern ocean: Constraints from riverine Mg isotope ratios. *Geochimica et Cosmochimica Acta*, *70*(18), A652. https://doi.org/10.1016/j.gca.2006.06.1215

Voigt, M., Pearce, C. R., Fries, D. M., Baldermann, A., & Oelkers, E. H. (2020). Magnesium isotope fractionation during hydrothermal seawater-basalt interaction. *Geochimica et Cosmochimica Acta*, *272*, 21–35. https://doi.org/10.1016/j.gca.2019.12.026

Wang, Z., Hu, P., Gaetani, G., Liu, C., Saenger, C., Cohen, A., & Hart, S. (2013). Experimental calibration of Mg isotope fractionation between aragonite and seawater. *Geochimica et Cosmochimica Acta*, *102*, 113–123. https://doi.org/10.1016/j.gca.2012.10.022

Wilson, S. A., Raudsepp, M., & Dipple, G. M. (2006). Verifying and quantifying carbon fixation in minerals from serpentine-rich mine tailings using the Rietveld method with X-ray powder diffraction data. *American Mineralogist*, *91*(8–9), 1331–1341. https://doi.org/10.2138/am.2006.2058

Wombacher, F., Eisenhauer, A., Böhm, F., Gussone, N., Regenberg, M., Dullo, W. C., & Rüggeberg, A. (2011). Magnesium stable isotope fractionation in marine biogenic calcite and aragonite. *Geochimica et Cosmochimica Acta*, *75*(19), 5797–5818. https://doi.org/10.1016/j.gca.2011.07.017

Xia, Z., Horita, J., Reuning, L., Bialik, O. M., Hu, Z., Waldmann, N. D., et al. (2020). Extracting Mg isotope signatures of ancient seawater from marine halite: A reconnaissance. *Chemical Geology*, *552*, 119768. https://doi.org/10.1016/j.chemgeo.2020.119768

Yamamoto, G. I., Kyono, A., & Okada, S. (2022). Thermal decomposition process of dypingite $Mg_5(CO_3)_4(OH)_2 \cdot 5H_2O$. *Materials Letters*, *308*, 131125. https://doi.org/10.1016/j.matlet.2021.131125

Young, E. D., Ash, R. D., Galy, A., & Belshaw, N. S. (2002). Mg isotope heterogeneity in the Allende meteorite measured by UV laser ablation-MC-ICPMS and comparisons with O isotopes. *Geochimica et Cosmochimica Acta*, *66*(4), 683–698. https://doi.org/10.1016/s0016-7037(01)00796-7

Zeyen, N., Benzerara, K., Beyssac, O., Daval, D., Muller, E., Thomazo, C., et al. (2021). Integrative analysis of the mineralogical and chemical composition of modern microbialites from ten Mexican lakes: What do we learn about their formation? *Geochimica et Cosmochimica Acta*, *305*, 148–184. https://doi.org/10.1016/j.gca.2021.04.030

Zhang, P., Huang, K., Luo, C., Chen, H., Bao, Z., Wen, H., & Zhang, X. (2021). Magnesium isotope fractionation during alkaline brine evaporation and implications for Precambrian seawater chemistry. *Chemical Geology*, *585*, 120565. https://doi.org/10.1016/j.chemgeo.2021.120565

Zheng, X., Zhang, M., Li, B., & Xu, C. (2002). *Salt lakes of China*. Science Press.

References From the Supporting Information

Ahmad, A., Jehangir, A., Yousuf, A. R., Shah, W. A., & Tanveer, A. (2020). Major ion chemistry of surface sediments of brackish endorheic lake Tso Moriri-A high altitude Ramsar site in western Himalaya. *Journal of Himalayan Ecology and Sustainable Development*, *15*, 41–57.

Barbiéro, L., de Queiroz Neto, J. P., Ciornei, G., Sakamoto, A. Y., Capellari, B., Fernandes, E., & Valles, V. (2002). Geochemistry of water and ground water in the Nhecolândia, Pantanal of Mato Grosso, Brazil: Variability and associated processes. *Wetlands*, *22*(3), 528–540. https://doi.org/10.1672/0277-5212(2002)022[0528:gowagw]2.0.co;2

Baumann, A., Förstner, U., & Rohde, R. (1975). Lake Shala: Water chemistry, mineralogy and geochemistry of sediments in an Ethiopian rift lake. *Geologische Rundschau*, *64*(1), 593–609. https://doi.org/10.1007/bf01820685

Bayly, I., & Williams, W. (1966). Chemical and biological studies on some saline lakes of south-east Australia. *Marine and Freshwater Research*, *17*(2), 177–228. https://doi.org/10.1071/mf9660177

Beinlich, A., & Austrheim, H. (2012). In situ sequestration of atmospheric CO_2 at low temperature and surface cracking of serpentinized peridotite in mine shafts. *Chemical Geology*, *332*, 32–44. https://doi.org/10.1016/j.chemgeo.2012.09.015

Bolou-Bi, E. B., Vigier, N., Poszwa, A., Boudot, J.-P., & Dambrine, E. (2012). Effects of biogeochemical processes on magnesium isotope variations in a forested catchment in the Vosges Mountains (France). *Geochimica et Cosmochimica Acta*, *87*, 341–355. https://doi.org/10.1016/j.gca.2012.04.005

Boros, E., & Kolpakova, M. (2018). A review of the defining chemical properties of soda lakes and pans: An assessment on a large geographic scale of Eurasian inland saline surface waters. *PLoS One*, *13*(8), e0202205. https://doi.org/10.1371/journal.pone.0202205

Borul, S. (2012). Study of water quality of Lonar Lake. *Journal of Chemical and Pharmaceutical Research*, *4*(3), 1716–1718.

Brasier, A., Wacey, D., Rogerson, M., Guagliardo, P., Saunders, M., Kellner, S., et al. (2018). A microbial role in the construction of mono lake carbonate chimneys? *Geobiology*, *16*(5), 540–555. https://doi.org/10.1111/gbi.12292

Brenna, B. L. (2016). *The chemical, physical, and microbial origins of Pleistocene cherts at Lake Magadi, Kenya Rift Valley* (Unpublished doctoral dissertation). University of Saskatchewan.

Cangemi, M., Censi, P., Reimer, A., D'Alessandro, W., Hause-Reitner, D., Madonia, P., et al. (2016). Carbonate precipitation in the alkaline lake Specchio di Venere (Pantelleria Island, Italy) and the possible role of microbial mats. *Applied Geochemistry*, *67*, 168–176. https://doi.org/10.1016/j.apgeochem.2016.02.012

Castanier, S., Bernet-Rollande, M.-C., Maurin, A., & Perthuisot, J.-P. (1993). Effects of microbial activity on the hydrochemistry and sedimentology of Lake Logipi, Kenya. In *Saline Lakes V* (pp. 99–112). Springer.

Coshell, L., Rosen, M., & McNamara, K. (1998). Hydromagnesite replacement of biomineralized aragonite in a new location of Holocene stromatolites, lake Walyungup, Western Australia. *Sedimentology*, *45*(6), 1005–1018. https://doi.org/10.1046/j.1365-3091.1998.00187.x

Deocampo, D. M. (2005). Evaporative evolution of surface waters and the role of aqueous CO_2 in magnesium silicate precipitation: Lake Eyasi and Ngorongoro Crater, northern Tanzania. *South African Journal of Geology*, *108*(4), 493–504. https://doi.org/10.2113/108.4.493

De Villiers, S., Dickson, J., & Ellam, R. (2005). The composition of the continental river weathering flux deduced from seawater Mg isotopes. *Chemical Geology*, *216*(1–2), 133–142. https://doi.org/10.1016/j.chemgeo.2004.11.010

Dinka, M. O. (2017). Analysing the temporal water quality dynamics of Lake Basaka, Central Rift Valley of Ethiopia. In *IOP Conference Series: Earth and Environmental Science* (Vol. 52, No. 1, p. 012057). IOP Publishing.

Fries, D. M., James, R. H., Dessert, C., Bouchez, J., Beaumais, A., & Pearce, C. R. (2019). The response of Li and Mg isotopes to rain events in a highly-weathered catchment. *Chemical Geology*, *519*, 68–82. https://doi.org/10.1016/j.chemgeo.2019.04.023

Fritz, B., Zins-Pawlas, M.-P., & Gueddari, M. (1987). Geochemistry of silica-rich brines from Lake Natron (*Tanzania*), géochimie des saumures riches en silice du lac Natron (*Tanzania*). *Sciences Géologiques, bulletins et mémoires*, *40*(1), 97–110. https://doi.org/10.3406/sgeol.1987.1753

Frondini, F., Vaselli, O., & Vetuschi Zuccolini, M. (2019). Consumption of atmospheric carbon dioxide through weathering of ultramafic rocks in the Voltri Massif (*Italy*): Quantification of the process and global implications. *Geosciences*, *9*(6), 258. https://doi.org/10.3390/geosciences9060258

Fukushi, K., Imai, E., Sekine, Y., Kitajima, T., Gankhurel, B., Davaasuren, D., & Hasebe, N. (2020). In situ formation of monohydrocalcite in alkaline saline lakes of the valley of Gobi lakes: Prediction for Mg, Ca, and total dissolved carbonate concentrations in Enceladus' Ocean and alkaline-carbonate ocean worlds. *Minerals*, *10*(8), 669. https://doi.org/10.3390/min10080669

Fussmann, D., von Hoyningen-Huene, A. J. E., Reimer, A., Schneider, D., Babková, H., Peticzka, R., et al. (2020). Authigenic formation of Ca–Mg carbonates in the shallow alkaline Lake Neusiedl, Austria. *Biogeosciences*, *17*(7), 2085–2106. https://doi.org/10.5194/bg-17-2085-2020

Galy, A., Bar-Matthews, M., Halicz, L., & O'Nions, R. K. (2002). Mg isotopic composition of carbonate: Insight from speleothem formation. *Earth and Planetary Science Letters*, *201*(1), 105–115. https://doi.org/10.1016/s0012-821x(02)00675-1

Gao, T., Ke, S., Wang, S. J., Li, F., Liu, C., Lei, J., et al. (2018). Contrasting Mg isotopic compositions between Fe-Mn nodules and surrounding soils: Accumulation of light Mg isotopes by Mg-depleted clay minerals and Fe oxides. *Geochimica et Cosmochimica Acta*, *237*, 205–222. https://doi.org/10.1016/j.gca.2018.06.028

Gaskova, O. L., Borzenko, S. V., & Shironosova, G. P. (2017). REE distribution during sedimentation in soda Lake Doroninskoye (Eastern Transbaikalia). *Procedia Earth and Planetary Science*, *17*, 694–697. https://doi.org/10.1016/j.proeps.2016.12.156

Gérard, E., De Goeyse, S., Hugoni, M., Agogué, H., Richard, L., Milesi, V., et al. (2018). Key role of alphaproteobacteria and cyanobacteria in the formation of stromatolites of Lake Dziani Dzaha (Mayotte, Western Indian Ocean). *Frontiers in Microbiology*, *9*, 796. https://doi.org/10.3389/fmicb.2018.00796

Gierlowski-Kordesch, E., & Kelts, K. (2006). *Global geological record of lake basins: Volume 1*. Cambridge University Press.

Gosselin, D. C., Sibray, S., & Ayers, J. (1994). Geochemistry of K-rich alkaline lakes, Western Sandhills, Nebraska, USA. *Geochimica et Cosmochimica Acta*, *58*(5), 1403–1418. https://doi.org/10.1016/0016-7037(94)90545-2

Hammer, U. T., & Forró, L. (1992). Zooplankton distribution and abundance in saline lakes of British Columbia, Canada. *International Journal of Salt Lake Research*, *1*(1), 65–80. https://doi.org/10.1007/bf02904952

Hecky, R. E., & Kilham, P. (1973). Diatoms in alkaline, saline lakes: Ecology and geochemical implications. *Limnology & Oceanography*, *18*(1), 53–71. https://doi.org/10.4319/lo.1973.18.1.0053

Hindshaw, R. S., Teisserenc, R., Le Dantec, T., & Tananaev, N. (2019). Seasonal change of geochemical sources and processes in the Yenisei River: A Sr, Mg and Li isotope study. *Geochimica et Cosmochimica Acta*, *255*, 222–236. https://doi.org/10.1016/j.gca.2019.04.015

Hussainy, S. U. (1969). *Ecological studies on some microbiota of lakes in western Victoria*. Department of Zoology, Monash University.

Immenhauser, A., Buhl, D., Richter, D., Niedermayr, A., Riechelmann, D., Dietzel, M., & Schulte, U. (2010). Magnesium-isotope fractionation during low-Mg calcite precipitation in a limestone cave–field study and experiments. *Geochimica et Cosmochimica Acta*, *74*(15), 4346–4364. https://doi.org/10.1016/j.gca.2010.05.006

Jirsa, F., Gruber, M., Stojanovic, A., Omondi, S. O., Mader, D., Körner, W., & Schagerl, M. (2013). Major and trace element geochemistry of Lake Bogoria and Lake Nakuru, Kenya, during extreme draught. *Geochemistry*, *73*(3), 275–282. https://doi.org/10.1016/j.chemer.2012.09.001

Johannesson, K. H., Lyons, W. B., & Bird, D. A. (1994). Rare Earth element concentrations and speciation in alkaline lakes from the western USA. *Geophysical Research Letters*, *21*(9), 773–776. https://doi.org/10.1029/94gl00005

Karasinski, J., Bulska, E., Wojciechowski, M., Halicz, L., & Krata, A. A. (2017). High precision direct analysis of magnesium isotope ratio by ion chromatography/multicollector-ICPMS using wet and dry plasma conditions. *Talanta*, *165*, 64–68. https://doi.org/10.1016/j.talanta.2016.12.033

Kaźmierczak, J., Kempe, S., Kremer, B., López-García, P., Moreira, D., & Tavera, R. (2011). Hydrochemistry and microbialites of the alkaline crater lake Alchichica, Mexico. *Facies*, *57*(4), 543–570. https://doi.org/10.1007/s10347-010-0255-8

Kimmig, S. R., Holmden, C., & Bélanger, N. (2018). Biogeochemical cycling of Mg and its isotopes in a sugar maple forest in Québec. *Geochimica et Cosmochimica Acta*, *230*, 60–82. https://doi.org/10.1016/j.gca.2018.03.020

Krám, P., Hruška, J., & Shanley, J. B. (2012). Streamwater chemistry in three contrasting monolithologic Czech catchments. *Applied Geochemistry*, *27*(9), 1854–1863. https://doi.org/10.1016/j.apgeochem.2012.02.020

Last, W. M. (1989). Sedimentology of a saline playa in the northern Great Plains, Canada. *Sedimentology*, *36*(1), 109–123. https://doi.org/10.1111/j.1365-3091.1989.tb00823.x

Lee, S. W., Ryu, J. S., & Lee, K. S. (2014). Magnesium isotope geochemistry in the Han River, South Korea. *Chemical Geology*, *364*, 9–19. https://doi.org/10.1016/j.chemgeo.2013.11.022

Li, L., Zhang, F., Jin, Z., Xiao, J., Gou, L.-F., & Xu, Y. (2020). Riverine Mg isotopes response to glacial weathering within the Muztag catchment of the eastern Pamir Plateau. *Applied Geochemistry*, *118*, 104626. https://doi.org/10.1016/j.apgeochem.2020.104626

Ma, L., Teng, F. Z., Jin, L., Ke, S., Yang, W., Gu, H. O., & Brantley, S. L. (2015). Magnesium isotope fractionation during shale weathering in the shale hills critical zone observatory: Accumulation of light Mg isotopes in soils by clay mineral transformation. *Chemical Geology*, *397*, 37–50. https://doi.org/10.1016/j.chemgeo.2015.01.010

Maddocks, G. (1967). The geochemistry of surface waters of the western district of Victoria. *Marine and Freshwater Research*, *18*(1), 35–52. https://doi.org/10.1071/mf9670035

Mavromatis, V., Prokushkin, A. S., Korets, M. A., Chmeleff, J., Mounic, S., & Pokrovsky, O. S. (2020). Weak impact of landscape parameters and rock lithology on Mg isotope composition of the Yenisey River and its tributaries. *Chemical Geology*, *540*, 119547. https://doi.org/10.1016/j.chemgeo.2020.119547

Mavromatis, V., Prokushkin, A. S., Pokrovsky, O. S., Viers, J., & Korets, M. A. (2014). Magnesium isotopes in permafrost-dominated Central Siberian larch forest watersheds. *Geochimica et Cosmochimica Acta*, *147*, 76–89. https://doi.org/10.1016/j.gca.2014.10.009

Mayfield, K. K., Eisenhauer, A., Santiago Ramos, D. P., Higgins, J. A., Horner, T. J., Auro, M., et al. (2021). Groundwater discharge impacts marine isotope budgets of Li, Mg, Ca, Sr, and Ba. *Nature Communications*, *12*(1), 1–9. https://doi.org/10.1038/s41467-020-20248-3

McClain, C., & Maher, K. (2016). Chromium fluxes and speciation in ultramafic catchments and global rivers. *Chemical Geology*, *426*, 135–157. https://doi.org/10.1016/j.chemgeo.2016.01.021

Mokgedi, L., Nobert, J., & Munishi, S. (2019). Assessment of lake surface dynamics using satellite imagery and in-situ data; case of Lake Ngami in North-West Botswana. *Physics and Chemistry of the Earth, Parts A/B/C*, *112*, 175–186. https://doi.org/10.1016/j.pce.2018.12.008

Namsaraev, Z. B., Zaitseva, S. V., Gorlenko, V. M., Kozyreva, L. P., & Namsaraev, B. B. (2015). Microbial processes and factors controlling their activities in alkaline lakes of the Mongolian plateau. *Chinese Journal of Oceanology and Limnology*, *33*(6), 1391–1401. https://doi.org/10.1007/s00343-015-4373-6

Opfergelt, S., Burton, K., Georg, R., West, A., Guicharnaud, R., Sigfusson, B., et al. (2014). Magnesium retention on the soil exchange complex controlling Mg isotope variations in soils, soil solutions and vegetation in volcanic soils, Iceland. *Geochimica et Cosmochimica Acta*, *125*, 110–130. https://doi.org/10.1016/j.gca.2013.09.036

Oskierski, H., Dlugogorski, B., Oliver, T., & Jacobsen, G. (2016). Chemical and isotopic signatures of waters associated with the carbonation of ultramafic mine tailings, Woodsreef Asbestos Mine, Australia. *Chemical Geology*, *436*, 11–23. https://doi.org/10.1016/j.chemgeo.2016.04.014

Pecoraino, G., D'Alessandro, W., & Inguaggiato, S. (2015). The other side of the coin: Geochemistry of alkaline lakes in volcanic areas. In *Volcanic lakes* (pp. 219–237). Springer.

Pogge von Strandmann, P. A. E., Burton, K. W., James, R. H., van Calsteren, P., Gislason, S. R., & Sigfússon, B. (2008). The influence of weathering processes on riverine magnesium isotopes in a basaltic terrain. *Earth and Planetary Science Letters*, *276*(1–2), 187–197. https://doi.org/10.1016/j.epsl.2008.09.020

Pogge von Strandmann, P. A. E., Opfergelt, S., Lai, Y.-J., Sigfússon, B., Gislason, S. R., & Burton, K. W. (2012). Lithium, magnesium and silicon isotope behaviour accompanying weathering in a basaltic soil and pore water profile in Iceland. *Earth and Planetary Science Letters*, *339*, 11–23. https://doi.org/10.1016/j.epsl.2012.05.035

Rawson, D. S., & Moore, J. (1944). The saline lakes of Saskatchewan. *Canadian Journal of Research*, *22*(6), 141–201. https://doi.org/10.1139/cjr44d-011

Reddy, M. M., & Hoch, A. (2012). Calcium carbonate nucleation in an alkaline lake surface water, Pyramid Lake, Nevada, USA. *Aquatic Geochemistry*, *18*(2), 95–113. https://doi.org/10.1007/s10498-011-9150-3

Reimer, A., Landmann, G., & Kempe, S. (2009). Lake Van, Eastern Anatolia, hydrochemistry and history. *Aquatic Geochemistry*, *15*(1), 195–222. https://doi.org/10.1007/s10498-008-9049-9

Riechelmann, S., Buhl, D., Schröder-Ritzrau, A., Riechelmann, D., Richter, D., Vonhof, H., et al. (2012). The magnesium isotope record of cave carbonate archives. *Climate of the Past*, *8*(6), 1849–1867. https://doi.org/10.5194/cp-8-1849-2012

Rosen, M. R., Miser, D. E., & Warren, J. K. (1988). Sedimentology, mineralogy and isotopic analysis of Pellet Lake, Coorong region, South Australia. *Sedimentology*, *35*(1), 105–122. https://doi.org/10.1111/j.1365-3091.1988.tb00907.x

Salem, S. M., & Gammal, E. S. A. E. (2018). Salt minerals at Wadi El Natrun saline lakes, Egypt. New implications from remote sensing data. *European Chemical Bulletin*, *7*(2), 72–80. https://doi.org/10.17628/ecb.2018.7.72-80

Samylina, O. S., & Zaytseva, L. V. (2019). Characterization of modern dolomite stromatolites from hypersaline Petukhovskoe Soda Lake, Russia. *Lethaia*, *52*(1), 1–13. https://doi.org/10.1111/let.12286

Schopka, H., Derry, L., & Arcilla, C. (2011). Chemical weathering, river geochemistry and atmospheric carbon fluxes from volcanic and ultramafic regions on Luzon Island, the Philippines. *Geochimica et Cosmochimica Acta*, *75*(4), 978–1002. https://doi.org/10.1016/j.gca.2010.11.014

Schuessler, J. A., von Blanckenburg, F., Bouchez, J., Uhlig, D., & Hewawasam, T. (2018). Nutrient cycling in a tropical montane rainforest under a supply-limited weathering regime traced by elemental mass balances and Mg stable isotopes. *Chemical Geology*, *497*, 74–87. https://doi.org/10.1016/j.chemgeo.2018.08.024

Stewart, M. K., Cameron, S., Hong, T., Daughney, C., Tait, T., & Thomas, J. T. (2003). Investigation of groundwater in the Upper Motueka River Catchment. *GNS Science Report*, *32*, 47.

Stober, I., Teiber, H., Li, X., Jendryszczyk, N., & Bucher, K. (2017). Chemical composition of surface-and groundwater in fast-weathering silicate rocks in the Seiland Igneous Province, North Norway. *Norwegian Journal of Geology/Norsk Geologisk Forening*, *97*(1), 63–94. https://doi.org/10.17850/njg97-1-04

Thompson, B. R. (1971). *The geology and hydrogeology of the Corangamite region* (Unpublished doctoral dissertation). The University of Melbourne.

Tipper, E. T., Calmels, D., Gaillardet, J., Louvat, P., Capmas, F., & Dubacq, B. (2012). Positive correlation between Li and Mg isotope ratios in the river waters of the Mackenzie Basin challenges the interpretation of apparent isotopic fractionation during weathering. *Earth and Planetary Science Letters*, *333*, 35–45. https://doi.org/10.1016/j.epsl.2012.04.023

Vidaković, D., Krizmanić, J., Dojčinović, B. P., Pantelić, A., Gavrilović, B., Živanović, M., et al. (2019). Alkaline soda Lake Velika Rusanda (Serbia): The first insight into diatom diversity of this extreme saline lake. *Extremophiles*, *23*(3), 347–357. https://doi.org/10.1007/s00792-019-01088-6

Warren, J. K. (1990). Sedimentology and mineralogy of dolomitic Coorong Lakes, South Australia. *Journal of Sedimentary Research*, *60*(6), 843–858.

Wimpenny, J., Burton, K. W., James, R. H., Gannoun, A., Mokadem, F., & Gíslason, S. R. (2011). The behaviour of magnesium and its isotopes during glacial weathering in an ancient shield terrain in west Greenland. *Earth and Planetary Science Letters*, *304*(1–2), 260–269. https://doi.org/10.1016/j.epsl.2011.02.008

Yadav, D., Sarin, M., & Krishnaswami, S. (2007). Hydrogeochemistry of Sambhar Salt Lake, Rajasthan: Implication to recycling of salt and annual salt budget. *Journal of the Geological Society of India*, *69*(1), 139.

Yan, L. X., Sun, M. P., Yao, X. J., Gong, N. G., Li, X. F., & Qi, M. M. (2018). Lake water in the Tibet Plateau: Quality change and current status evaluation. *Acta Scientiae Circumstantiae*, *38*(3), 900–910.

Yuretich, R. F., & Cerling, T. E. (1983). Hydrogeochemistry of Lake Turkana, Kenya: Mass balance and mineral reactions in an alkaline lake. *Geochimica et Cosmochimica Acta*, *47*(6), 1099–1109. https://doi.org/10.1016/0016-7037(83)90240-5

Zeyen, N., Benzerara, K., Li, J., Groleau, A., Balan, E., Robert, J. L., et al. (2015). Formation of low-T hydrated silicates in modern microbialites from Mexico and implications for microbial fossilization. *Frontiers of Earth Science*, *3*, 64. https://doi.org/10.3389/feart.2015.00064

Zhang, H., Jiang, X. W., Wan, L., Ke, S., Liu, S. A., Han, G., et al. (2018). Fractionation of Mg isotopes by clay formation and calcite precipitation in groundwater with long residence times in a sandstone aquifer, Ordos Basin, China. *Geochimica et Cosmochimica Acta*, *237*, 261–274. https://doi.org/10.1016/j.gca.2018.06.023

Zhao, T., Liu, W., Xu, Z., Sun, H., Zhou, X., Zhou, L., et al. (2019). The influence of carbonate precipitation on riverine magnesium isotope signals: New constrains from Jinsha River Basin, Southeast Tibetan Plateau. *Geochimica et Cosmochimica Acta*, *248*, 172–184. https://doi.org/10.1016/j.gca.2019.01.005

Zheng, M., Xiang, J., Wei, X., & Zheng, Y. (1989). *Saline lakes on the Qinghai-Tibet Plateau*. Science and Technology Press.

Zheng, X. (1992). *Salt lakes in inner Mongolia, China*. Science and Technology Press.

Zheng, X., & Lu, Y. (1995). Salt lakes and carbonate origin in Hailar Basin. *Journal of Salt Lake Science*, *3*, 1–10.

Zheng, X., Tang, Y., Xu, B., Li, C., & Zhang, B. (1988). *Salt lakes in Tibet*. Science and Technology Press.